AFAL-TR-76-147

SECURITY CLASSIFICATION OF THIS PAGE *(When Data Entered)*

REPORT DOCUMENTATION PAGE		READ INSTRUCTIONS BEFORE COMPLETING FORM
1. REPORT NUMBER AFAL-TR-76-147	2. GOVT ACCESSION NO.	3. RECIPIENT'S CATALOG NUMBER
4. TITLE *(and Subtitle)* Research on Crystal Growth and the Optical and Magneto-Optical Properties of Semiconductors.		5. TYPE OF REPORT & PERIOD COVERED Final Report 1 Jul 1964 — 30 Jun 1974
		6. PERFORMING ORG. REPORT NUMBER
7. AUTHOR(s) Cole W. Litton		8. CONTRACT OR GRANT NUMBER(s)
9. PERFORMING ORGANIZATION NAME AND ADDRESS Air Force Avionics Laboratory Bldg 450, WPAFB, OH 45433		10. PROGRAM ELEMENT, PROJECT, TASK AREA & WORK UNIT NUMBERS 78850104
11. CONTROLLING OFFICE NAME AND ADDRESS Air Force Avionics Laboratory Bldg 450, WPAFB, OH 45433		12. REPORT DATE August 1976
		13. NUMBER OF PAGES 77
14. MONITORING AGENCY NAME & ADDRESS*(if different from Controlling Office)*		15. SECURITY CLASS. *(of this report)* Unclassified
		15a. DECLASSIFICATION/DOWNGRADING SCHEDULE

16. DISTRIBUTION STATEMENT *(of this Report)*

Approved for public release; distribution unlimited

17. DISTRIBUTION STATEMENT *(of the abstract entered in Block 20, if different from Report)*

18. SUPPLEMENTARY NOTES

19. KEY WORDS *(Continue on reverse side if necessary and identify by block number)*

Crystal Growth;	Infrared Cyclotron Resonance;	Solar Cells
Optical Properties;	Polarons Spin-Flip Raman Scattering;	
Magneto-Optical Properties;	II-VI Compound Semiconductors;	
Excitons;	III-V Compound Semiconductors;	
Defects;	Infrared Laser Windows;	

20. ABSTRACT *(Continue on reverse side if necessary and identify by block number)*

This report covers the research performed during the period from 1 July 1964 to 30 June 1974 by scientists from the Group "Research on Crystal Growth and the Optical and Magneto-Optical Properties of Semiconductors" and was performed in the Solid State Physics Research Laboratory of the Aerospace Research Laboratories Wright-Patterson Air Force Base, Ohio, under Project 7885, Task 01. Some highlights and significant achievements of the research program in the areas of crystal growth, optical and magneto-optical properties of II-VI and III-V semi-

CONT.

DD $_{1\ JAN\ 73}^{FORM}$ 1473   EDITION OF 1 NOV 65 IS OBSOLETE

conductors, and device oriented research are discussed qualitatively. The crystal growth program is discussed in terms of defect production and purification in the II-VI semiconducting compounds, particularly CdS, CdSe, ZnS, ZnO, ZnSe, ZnTe, CdTe and α-HgS. The optical and magneto-optical properties of the II-VI compounds are discussed either with respect to characterization of their fundamental optical and magneto-optical parmeters, or to characterization of the defect and impurity structure of these materials. Experimental values of some of the more important physical constants of these materials, such as bandgaps, electron and hole effective masses and g-factors, exciton parameters, dielectric constants and refractive indices, are summarized in the various tables of the report. The electronic defect and impurity structure of these materials is discussed in a general way, more with respect to analytical approach and method, than to the identification of specific impurities and defects. Device oriented research is discussed mainly in connection with CdS solar cell research and development and, the growth and characterization of high-power infrared laser window materials.

ACCESSION for

NTIS	White Section	☑
DDC	Buff Section	☐
UNANNOUNCED		☐
JUSTIFICATION		

BY
DISTRIBUTION/AVAILABILITY CODES

| Dist. | AVAIL. and/or SPECIAL |
| A | |

FOREWORD

    This Final Technical Report describes the basic and applied research under Project 7885, Task 01, entitled "Research on Crystal Growth and the Optical and Magneto-Optical Properties of Semiconductors", during the period from 1 July 1964 to 30 June 1974. The report briefly summarizes the results of extensive experimental and theoretical investigations of the optical and magneto-optical properties of compound semiconductors, mostly the Group II-VI compounds, which were performed in the Aerospace Research Laboratories, Wright-Patterson Air Force Base, Ohio, under the above Task/Project. These investigations were aimed primarily toward a complete characterization of the electronic energy band parameters and defect status in these materials by means of high-resolution optical and magneto-optical spectroscopy. The report also briefly summarizes the techniques of vapor phase crystal growth which were used to synthesize the crystal specimens employed in these investigations. Exploitation of compound semiconductors for device applications was the ultimate objective of the research.

    Although a number of scientists contributed to the research over a period of several years, the principal investigators and leaders of the Task Effort were the following:
        D. C. Reynolds, Principal Investigator
        C. W. Litton, Principal Investigator
        T. C. Collins, Research Scientist
        L. C. Greene, Research Scientist
D. C. Reynolds was the principal investigator during the period 1 July 1964 to 1 August 1971; C. W. Litton served as principal investigator from 1 August 1971 to 30 June 1974.

    Most of the research has been reported in a series of papers published in the scientific and engineering literature, the more important of which are referenced in the Appendix at the end of Section VII (List of Publications).

TABLE OF CONTENTS

TABLE OF CONTENTS

AFAL-TR-76-147

SECTION I

INTRODUCTION

The primary objective of this task has been the optical and magneto-optical characterization of the intrinsic and extrinsic properties of compound semiconductors, primarily from the II-VI group of crystalline materials. Active over a period of some ten years (from July 1964), the major goal of the task effort was to extend the laboratory's early work on semiconductor optical properties by 1) initially concentrating its basic research efforts on the complete characterization of the fundamental optical and magneto-optical properties of wide bandgap semiconductors and then 2) to extend the optical and magneto-optical studies to a complete characterization of the extrinsic properties of these materials. As semiconductor science and device technology have shown in the past, development of the Silicon and Germanium transistors being good cases in point, it was necessary that the first step be achieved before the second could be realized. As defined here fundamental or intrinsic properties refer to those electronic energy band states and the other parametric constants, such as charge carrier effective mass, free exciton parameters, phonon states and energies, dielectric functions, refractive indices, etc., which belong to the crystalline lattice of the pure crystal, i.e., uniquely defined and reproducibly measurable properties; extrinsic properties, on the other hand, refer to electronic defect properties, arising from the presence of both foreign impurity atoms and host lattice (stoichiometric) defects in the pure crystal lattice. One obvious goal of this task has been to establish the optical, magneto-optical and electronic device potential of the II-VI compounds for electromagnetic devices which are required in Air Force systems, such as ultraviolet, visible and infrared detectors, photoconductors, image detectors and intensifiers, energy converters and power sources (solar batteries), field effect transistors, micro-electronic circuit arrays, microwave oscillators and generators, integrated optical circuit elements, junction diodes (rectifiers), light emitting diodes, laser tuning elements and parametric oscillators, acousto-electric and electro-optic elements, acoustic delay line elements, high power laser window materials, etc. In order to achieve this ultimate goal, it was first necessary to pursue a rather extensive in-house program of vapor phase and melt crystal growth of the II-VI compounds in order to maintain close control over crystal quality and defect production and particularly to minimize contamination by foreign impurities. It was also absolutely essential that the electronic impurity or defect state of these materials be completely understood and completely characterized, not only with respect to what foreign impurities and native defects were present in undoped, as-grown crystals, but also the concentrations of these residual impurities and defects and their effect on the intrinsic energy band parameters of the material. As part of this characterization

1

effort it was necessary to establish control of the impurity and defect structure in a given material by introducing known donor and acceptor impurities and defects through controlled doping experiments, mostly during crystal growth but also via controlled thermal diffusion, and then to develop optical and magneto-optical spectroscopic techniques to monitor the change in defect structure. As a consequence of these spectroscopic studies, all of the fundamental properties of the wide bandgap II-VI compounds have been carefully measured and defined and the electronic impurity or defect state is also well understood, in virtually all of these materials. The validity of the spectroscopic results is now well established, not only because of their close agreement with those of other methods (when available), but also because of their wide acceptance in the published scientific and engineering literature, over the past decade and more. The optical spectroscopy and characterization studies are summarized briefly in the various sections of this report; further details can be obtained from the pertinent published papers listed in the Appendix at the conclusion of the report. During the course of this task effort, several important "firsts" in semiconductor physics were achieved and these will be discussed briefly in the last two sections of the report.

The technique of high-resolution optical absorption, reflection and photoluminescence spectroscopy (at bandgap photon energies) is not only an extremely powerful tool for the analysis and study of intrinsic energy band parameters of semiconductors, as well as their impurity and defect states, but has also generally proven to be the best technique available for this purpose. Intrinsic or free exciton formation is observed in most well-formed, wide-bandgap crystal structures, under optical excitation at cryogenic temperatures, and such free excitons have proven to be a very powerful tool for probing the intrinsic band structure of semiconductors; by the same token, bound exciton complexes have proven to be an equally powerful tool for probing the impurity and defect structure of several of these semiconductor materials. The fact that the optical transitions arising from both free and bound exciton formation fall at photon energies near the bandgap makes exciton spectroscopy an even more attractive technique for the wide bandgap II-VI materials, since their bandgap spectral regions (ultraviolet to near infrared) fall at wavelengths for which extremely sensitive and fast radiation detectors (including photographic emulsions) are readily available. In conjunction with theoretically calculated energy band structure, the effective mass approximation and high magnetic fields (magneto-optical spectroscopy), optical bandgap spectroscopy usually yields far more useful information regarding the intrinsic and extrinsic properties of semiconductors than do alternative analytical techniques, such as electrical transport measurements, EPR, NMR, mass and emission spectroscopy, auger spectroscopy and several other standard techniques. Moreover, the spectroscopic technique is much more economical, in respect of

both experimental resources and the time required for analysis, than are most of the alternative analytical techniques which are available to the semiconductor physicist and engineer.

Actually, bandgap exciton spectroscopy is closely related to another spectroscopic resonance technique which has been widely used to probe the intrinsic band structure of both wide and narrow bandgap semiconductors. This technique, usually referred to collectively as interband or intraband infrared cyclotron resonance and originally developed at microwave frequencies, has been extensively employed in the measurement of charge carrier effective masses in semiconductors at high symmetry points in the Brillouin Zone and yields what are probably the most precise values of these parameters which have been determined to date. It has also been used to probe the shape of conduction and valence bands and to measure precisely the magnitude of the electron-phonon interaction in polar semiconductors. The intraband cyclotron resonance technique has been extended in recent years to studies of shallow donor and acceptor impurity resonances (Zeeman Spectroscopy) at far infrared frequencies and high magnetic fields, mostly since the advent of high-resolution Fourier transform spectroscopy (interferometry) and particularly since the advent of far infrared molecular gas lasers which radiate at submillimeter wavelengths. The technique of far infrared Zeeman spectroscopy of impurities and defects is usually referred to as submillimeter magneto-spectroscopy. It has proven to be an extremely sensitive and powerful technique for analyzing the defect structure of semiconductors and for detecting the presence of different donors and acceptors of nearly equal binding energy (chemical shifts) in high mobility samples, particularly when the cross-modulation technique (photoconductive signal detection) is employed. In this mode as few as five impurity electrons out of some $10^{12}/cm^3$ can be detected. Zeeman spectroscopy of excitons at the bandgap and submillimeter magneto-spectroscopy are actually complementary spectroscopic techniques; one can sometimes be used to advantage instead of the other and both have been employed in the semiconductor characterization studies of this task effort. One recent example of the power of the spectroscopic technique can be seen in the following: For more than a decade, many experimental attempts have been made to determine precisely the magnitude of the electron-phonon scattering interaction due to large polaron formation in moderately to highly polar semiconductors and thereby establish the validity of Frohlich's continuum model and his electron-phonon interaction theory. Many of these attempts employed electrical transport measurements or related techniques and all proved either unsuccessful or inconclusive. In recent work of this task effort, conduction-band-electron cyclotron resonance absorption measurements were performed at submillimeter wavelengths on high-mobility specimens of moderately polar n-type CdTe and the experimental results (polaron-induced shifts in cyclotron frequency and electron mass) were, for the first time, in excellent quantitative agreement with the predictions

3

of the one-phonon quantum mechanical theory of the Frohlich electron-phonon scattering interaction over a wide range of cyclotron frequencies and fields.

The task was divided into essentially three parallel efforts:

1) Crystal Growth and Preparation
2) Optical Properties
3) Magneto-Optical Properties

These three separate but interdependent efforts are treated in separate sections of the report under the same titles. This is followed by a separate section which discusses several device oriented research projects and another which briefly summarizes the significant achievements of the task. The report concludes with a summary of the experimental findings together with recommendations for future research and device applications.

SECTION II

CRYSTAL GROWTH AND PREPARATION

1. INTRODUCTION

A substantial part of this task effort (about 50%) was de-
voted to the growth and preparation of the Group II - VI crystals
and to research aimed at improving the purity and quality of both
single and polycrystals of these materials; the effort included
research on improved methods of crystal growth, such as novel
furnace designs, precise temperature measurement and control,
ultra-purification of raw materials and controlled impurity doping
techniques. Depending on the purpose for which they were intended,
crystals were grown in two basically different forms: 1) large,
single and polycrystalline ingots (up to 5-6 in.^{3} in volume),
and 2) thin, high-quality, hexagonal platelets up to 1cm^2 in
cross-section. Virtually all of the wide bandgap II - VI compounds,
such as CdS, ZnS, ZnO, CdSe, ZnSe, ZnTe, CdTe and HgS, were grown
in one of these forms or the other during the course of this program.
Most of the II - VI compounds crystallize in the zincblende (cubic)
structure, but several crystallize in the hexagonal modification
and these will be identified below. The bulk crystal growth effort
was aimed primarily at the production of large, bulk-single-crystals
for direct device applications, as well as for the research needs
of the entire Laboratory research program, while the platelet-
crystal growth effort was directed primarily toward experimen-
tation to improve the chemical purity and structural quality of
the II - VI compound crystals. The platelet growth effort also
included a program of high-resolution, magneto-optical spectro-
scopy (mostly bound exciton spectroscopy) which was used as an
analytical tool for the identification of residual concentrations
of chemical impurities and defects in these materials. This
program on the magneto-optical spectroscopy of defects and im-
purities in platelet crystals was begun in the early 1960's by
Reynolds, Litton and Collins (summarized in several papers on
bound exciton Zeeman spectroscopy referenced in the Appendix
of this report); it was continued by Greene, starting in the
mid-1960's, primarily for the purpose of studying and identify-
ing specific kinds of electronic defects commonly encountered in
CdS, CdSe and CdS:Se, such as those introduced by the alkali
metals and the halogens (see L. C. Greene, ARL Final Report No.
TR 75-0094). The platelet type crystals (CdS, CdSe, ZnS and ZnO)
were chosen for the impurity and defect studies because they could
be grown with stable and reproducible defect, structure and
because they proved to be excellent general models of the defect
structure for all of the II - VI compounds. Many of the funda-
mental optical properties (discussed in the Introduction, Section I)
were also first measured and defined in the platelet crystals

because of their high-purity and high optical quality. The details of both bulk and platelet crystal growth techniques have been given in a review by Reynolds, Ref. 5, Appendix of this report, and are summarized briefly below.

2. BULK CRYSTALS

Single crystals of the wide bandgap II - VI compounds were grown by two principal methods

(1) Vapor phase sublimation of the compound in either static or gas flow systems and,

(2) High pressure melt-growth in modified Bridgman systems.

The polycrystalline infrared laser window specimens of ZnSe and ZnTe discussed in Section V were also grown by the vapor phase sublimation technique. Both vapor phase sublimation and high pressure melt furnaces were employed in the growth of the CdS, CdSe, ZnO, ZnS and CdTe single crystals whose optical and magneto-optical properties are summarized in Sections III and IV. Most of the II - VI compounds undergo sublimitation at high temperature and do not melt at atmospheric pressure. The exceptions are CdTe, HgSe, HgTe and HgCd:Te (and under certain circumstances, HgS) which can be grown from the melt at atmospheric pressure. In fact, the highest mobility CdTe crystals ever grown have been crystallized from the melt, using the techniques of traveling solvent, modified Bridgman and vertical zone melting. For example, the high mobility CdTe crystals ($\mu_e \sim 10^5 cm^2$/v-sec at 35 degrees K) employed in the polaron cyclotron and impurity resonance measurements discussed in Section IV were grown from low pressure metals. High pressure melt growth is often employed when impurity doping is required in the II - VI compounds, although the crystalline perfection of such crystals is not as high as that of crystals grown by vapor transport. This is particularly true for CdS, CdSe, ZnS and ZnO, and to a lesser extent for ZnSe and ZnTe. But it is usually possible to obtain a more uniform distribution of dopant in pressure-melt-grown crystals and to overcome the impurity segragation problem, often common to vapor-grown-crystals.

All of the vapor phase crystal furnaces employed for this sublimation growth of the II - VI crystals were designed and constructed in ARL. The single and multiple zone furnaces employed for this purpose were similar in principle to the original design of Reynolds and Czyzak. In a typical single zone furnace, thermal insulation is achieved with firebricks which surround the mullite-ceramic furnace liner tube. Six SiC heating elements

(rods) are positioned radially around the mullite tube and run the length of the furnace. In this arrangement, a hot zone approximately 18 inches long is developed at the center of the furnace. Measurement of the temperature gradient along the furnace length shows the temperature profile to be parabolically-shaped, with the hottest point lying at the center. Temperature control is maintained with a proportional **temperature controller** in conjunction with a Pt - Pt 0.13 Rh thermocouple, whose hot junction is positioned at the center of the furnace, adjacent to the external ceramic furnace tube. The growth chamber is provided within the inner quartz liner tube (approximately 2 - inch diameter) which is described below.

All of the bulk vaporgrown II - VI crystals discussed in this report were grown by the method of Reynolds, Czyzak and Greene which was first used in the late 1940's and early 1950's for the growth of CdS and ZnS. The method is essentially a static one employing an inert gas atmosphere. In the present versions of this method, the crystal powder charge is placed within two tele-scoping quartz tubes, one end of each tube being fitted with a roughened quartz seed plate. The quartz tubes are then pushed together, creating a chamber approximately six inches long for the powder charge, which ranges between 200 - 250 gms, depending upon the final crystal size desired. The quartz tube arrangement is then placed within the mullite furnace tube and positioned such that the charge lies at the maximum in the temperature profile. One end of the mullite tube is permanently closed and the other is sealed with a rubber stopper containing glass tube exhaust and inlet ports. The system is then evacuated with a mechanical pump and, while still under vacuum, the charge is fired (sintered) at approximately 800 degrees C for at least an hour. After firing, the system is purged several times with pure argon. Finally, the system is filled with argon and sealed. The furnace temperature is then raised to a point slightly above the sublimation tem-perature of the powder charge where it is maintained for the duration of the growth period. Typical sublimation temperatures are approximately 1300 degrees C for CdS; 1240 degrees C for CdSe; 1340 degrees C for ZnSe; and 1180 degrees C for CdTe. Hot subliming vapors from the powder charge are then deposited on the colder quartz seedplates which form the nucleation sites for single crystal growth. Typical temperature gradients maintained between the charge and seedplate were approximately 50 degrees C for CdS and ZnSe, and in the range of 30 - 40 degrees C for CdTe and CdSe. Approximately seven days are required for the growth of large boules of CdS, CdSe and ZnSe; 10 days for CdTe. At the completion of growth, the system is slowly returned to room tem-perature in order to prevent cracking of the single crystal boules

7

due to the differential thermal contraction between the crystal ingot and the quartz tube and seedplate to which it is attached. A similar version of this same system was also used to synthesize the large ZnSe and ZnTe single and polycrystalline infrared laser window cyrstals (discussed in Section V). In this case the quartz tubes and seedplates were coated with pyrolytic graphite in order to prevent sticking of the crystals to the growth chamber surfaces and thereby prevent cracking of the ingots during cool-down.

The vapor phase furnace was used to grow several of the high-purity, n-type CdS bulk specimens employed in the spin-flip-Raman scattering measurements summarized in Section IV. As grown, these crystals were usually of very high resistivity. In order to lower their resistivities, the crystals were sealed in quartz ampules and baked in a Cd atmosphere for periods of 24 to 36 hours. Following this procedure, specimens with room temperature mobilities 100 cm/v-sec and resistivities in the range of 1 to 0.01 ohm-cm could be obtained. Such specimens had room-temperature carrier concentrations in the range of 1×10^{17} to a few times 10^{18}/cm. Room temperature carrier concentrations in this range were required in order to achieve the low-temperature electron concentrations required for the spin-flip-Raman scattering measurements. Similar rocedures were also applied to the CdSe and CdTe vapor-grown specimens used in the light scattering experiments. Frequently, however, one finds that the vapor growth of pure CdTe yields p-type crystals of slightly non-stoichiometric composition, owing to the loss of Cd during high temperature sublimation. This effect has also been observed and can be a problem in the conventional low-pressure, melt-growth of CdTe. When the resistivity of such p-type crystals is not extremely high, they can be type-converted by baking in a Cd atmosphere and, occasionally, moderately low-resistivity, n-type material can be produced. Similar procedures were also applied to moderately-low-resistivity, as grown n-CdTe laser window specimens. The resistivity of such specimens could be increased to relatively high values by the compensation produced by baking in a Te atmosphere, thereby reducing their infrared radiative absorption losses to acceptable values for the window applications.

Several of the CdS, CdSe and ZnSe specimens employed in the spin-flip-Raman scattering studies were grown in a commercially-built, pressure-melt furnace, provided by the Eagle Pitcher Co. All of the Raman specimens grown by this method were donor-doped (with either Cl or Br) to concentration in the range of 1 to 100 ppm. The dopants were provided by various salts, mixed in the initial charge. Operating at pressures in the range of 1500 to 2000 psi and at temperatures somewhat lower than those required for vapor phase growth, n-type crystals of CdS, CdSe and ZnSe were grown over periods of several days. The pressure-melt furnace

was also used to grow CdS, ZnS, ZnSe and ZnTe crystals doped
with transition metal and rare earth ions which were used for
various research studies within the laboratory, particularly
spectroscopic, magneto-resistance and thermal conductivity char-
acterization studies of such impurities.

The thin (7 - 25μm thick) InAs epi-layer specimens employed
in the resonant polaron coupling studies and in the magneto-
spectroscopic studies (cyclotron resonance) of the shallow donor
electron were grown epitaxially in a three-zone, continuous-
hydrogen-flow, open-tube type epi-layer furnace of the type designed
and operated by McCarthey and Cronin. The epi-layers were
grown on Cr-doped, semi-insulating GaAs substrates. Bulk InAs
specimens were also employed in the cyclotron resonance mea-
surements and these were pulled from the melt. Some of the InAs
epi-layers were grown by the author and others were obtained
from various commercial sources and laboratories.

3. PLATELET CRYSTALS

Of the 12 chalcogenides of Zn, Cd and Hg, only CdS, CdSe,
ZnS and ZnO readily crystallize in the wurtzite hexagonal
structure, and it is only from these materials that the thin,
high-quality, platelet type crystals can be grown by vapor
phase sublimation; most of the others, such as CdTe, ZnTe and
ZnSe, normally crystallize in the zincblende cubic structure.

A modified version of the single zone vapor phase furnace
described above was originally employed for the growth of the
high-quality CdS, CdSe and ZnO platelets whose intrinsic and
bound exciton spectra are discussed in Sections III and IV.
In this dynamic system, the crystal vapor is transported across
a temperature gradient by means of an argon flow and is deposited
upon the sharp edges of a radially-cut quartz cylinder of small
diameter. Nucleation occurs at the sharp edges of the cylinder,
producing high-quality platelets as thin as 0.5 to 50 μm, with
cross sections up to 1cm2, and thicker platelets of lower quality
ranging up to 1000 m thick. Actually, a considerably more
sophisticated three-zone vapor furnace was used for the more
recent platelet growth of CdS and CdSe, but the basic vapor
phase technique remains essentially the same.

Platelet crystals grow predominantly in the direction of
their hexagonal c-axes and are bounded by natural crystal planes.
The very thin platelets also have the flexibility and crystalline
perfection of a whisker, indicating a very low defect concen-
tration. In fact, some of the very thin platelets of CdS show

no visible photoluminescence under intense optical excitation, indicating a very low concentration of optically active impurities and defects. Somewhat surprisingly, perhaps, the platelet crystals can also be grown to a stoichiometric excess of Cd and S. High purity platelets with excess Cd show a characteristic neutral donor complex, and those containing excess S show a neutral acceptor complex, as determined from Zeeman studies of their bound exciton photoluminescence spectra at temperatures 1 to 4 degrees K. This will be discussed further in Section IV.

4. SPECIMENT PREPARATION: CUTTING AND POLISHING

The optical, electrical, thermal and other semiconductor specimen preparation requirements of the entire laboratory were serviced by a part of this task effort. For example, optical transmission, reflection and photoluminescence specimens were cut from as-grown crystal ingots into many different geometries for many different types of scientific experiments, as well as for optical device applications. Crystal cutting was accomplished by means of diamond wire saws and cutting wheels. Often, it was also required that semiconductor specimens have their crystallographic axes and planes spacially oriented with respect to the specimen faces and surfaces; this was accomplished by means of x-ray diffraction measurements prior to cutting the specimen. The faces of optical specimens were ground and polished by standard lapidary techniques (automated lapping machines) and were typically polished to mirror-like finishes, through a series of wet-laps with successively finer abrasives, such as various grades of Al_2O_3 powder. Chemically polished specimens were also prepared, and, when required, specimen surfaces were chemically cleaned and roughened or polished with special etchants. Specimens of many different semiconductor materials were prepared during the course of this effort, not only the wide bandgap II-VI compounds, but also many of the III-V's, and Si and Ge as well. Often such specimens were required for special experimental purposes, such as infrared filters, transmission windows, and optical lenses, that could not be acquired commercially. Specimens were also prepared for special in-house projects, such as the small chips and wafers of doped ZnSe and ZnS required for the fabrication of light emitting diodes, as well as the optically polished specimens of ZnSe and ZnTe required for both in-house and contract programs on the development of optical waveguides and integrated optical circuit elements. As part of the Air Force High Power Infrared Laser Window Materials Program, which began early in 1971, a large number of CdSe, CdTe, ZnSe, ZnTe and ZnSe:Te laser window crystals were cut, polished

10

and otherwise prepared for optical transmission testing (absorption coefficient measurements) in the joint AF Materials Lab - AF Weapons Lab program. Most of these specimens were grown in-house, but a few were provided from various external contract programs. In fact, surface polishing techniques were developed especially for these window specimens in order to minimize their surface scattering and absorption losses. Small optical specimens of the window materials were also prepared for photoluminescence spectroscopic studies of the impurities and defects which they contained. The spectroscopic studies of the laser window materials were performed as a part of the basic task effort, but will be discussed separately under Section V.

SECTION III

OPTICAL PROPERTIES

1. INTRODUCTION

In addition to their interesting electrical properties, semiconductors also absorb, reflect, scatter, disperse and radiate light, and, in general, interact strongly with the electromagnetic radiation field. For this reason, many of their fundamental properties, such as energy bandgaps, activation energies, effective mass parameters, dielectric functions, refractive indices and lattice vibrational frequencies, can be determined from optical experiments, particularly from their optical spectra. As used here, the term "optical" refers to a broad region of the electromagnetic spectrum, ranging from the vacuum ultraviolet to the far infrared. Over the past two decades, optical spectroscopy has been increasingly employed for the study and measurement of semiconductor properties and has ultimately become a very powerful experimental tool. Some of the earliest determinations of the bandgaps in Ge and Si were made from measurements of their spectral transmission and reflectivity in the near infrared, and these measurements led ultimately to a better understanding of the indirect-allowed optical transitions and the off-axis conduction band minima in these important semiconductor materials which crystallize in the diamond structure. During the past ten years, optical spectroscopy has also become a very powerful tool for the study and characterization of electronic defects and impurities (bound states) in semiconductors. Much of our present understanding of the fundamental energy band structure in semiconductors, particularly in the II - VI and III - V compounds and in Ge and Si, has come through detailed studies of their intrinsic optical spectra, and there is still much to be learned from spectroscopic studies of impurities and defects in these materials.

In this section we shall deal with those intrinsic and extrinsic semiconductor parameters which can be measured and studied from optical spectra in the absense of a magnetic field; the effect of an externally applied magnetic field on these parameters will be treated separately under Magneto-Optical Properties in Section IV. In semiconductor optical spectra, virtually all of the spectral features arising from the optical transitions (electronic and lattice) sharpen markedly upon cooling to cryogenic temperatures. In fact, many of the important optical transitions which characterize

the quantum states of a semiconductor can only be observed
at very low temperatures (near 4.2 degrees K). This is caused,
in part, by a reduction in the various scattering mechanisms
which are dominant at room temperature and by a reduction in
the thermal spread of the quantum levels with respect to the
energy of the optical transition ($h\omega>>KT$). By measuring the
optical and magneto-optical spectra as a function of temperature,
a great deal of additional information about the intrinsic and
extrinsic properties of semiconductors can be obtained, partic-
ularly with regard to free electron and hole populations,
impurity concentrations and the oscillator strengths of the
optical transitions. For this reason, most of the semiconductor
optical spectra discussed here were measured as a function
of temperature, usually in the range of 1.2 to 4.2 degrees K
and rarely above 100 degrees K. Exciton spectra, e.g., are not,
observed in most of the II-VI compounds at temperatures much
above 10 degrees K, owing to the small binding energy of these
quasiparticles. Unless otherwise specified, all of the spectral
data discussed in this report were obtained at temperatures
between 1.2 and 4.2 degrees K.

2. EXPERIMENTAL APPROACH

In addition to unique crystal-growth facilities for the
II-VI compounds (vapor phase and pressure-melt furnaces), the
laboratory is also uniquely equipped to perform high-
resolution absorption, reflection and emission spectroscopy
in semiconductors, over a wide range of cryogenic temperatures.
Several cryogenic Dewars, with provision for immersion curling
of semiconductor optical specimens to temperatures as low as
1.2 degrees K, were employed in the spectral measurements, and
optical cryostats capable of operating between 10 and 300
degrees K were also available for specimen cooling. High-
resolution spectral analysis of the light transmitted, reflected,
emitted and scattered by the semiconductor specimens was
achieved with several modified Bausch and Lomb grating spectro-
graphs of 2 meter focal length, equipped with f/16 optics and
large 4" x 5", 55,000 lines/inch diffraction gratings. The
high-resolution grating spectrometers had a spectral range from
2000Å to about 2 μm wavelength and were thus extremely useful
for bandgap spectral studies in all of the II-VI compounds
considered in this report. These spectrographs were capable
of a limiting spectral resolution of 0.08cm^{-1} ($1 \times 10^{-5}\text{eV}$)
at the narrowest slit widths. The spectrally analyzed
radiation was detected with high-speed photographic emulsions
and with photoelectronic detectors. Continuous radiation

(sources) was provided by high-intensity tungsten lamps and by
high-pressure zirconium lamps; photoluminescence excitation
was provided by filtered U-V sources (high-pressure Hg arc
lamps) and by rare gas ion laser sources.

Infrared absorption and photoconductivity spectral mea-
surements were performed in a far infrared, vacuum-grating
spectrometer capable of providing monochromatic radiation from
the visible out to 120 μm wavelength. Designed and constructed
in-house, this monochromator is particularly well suited for
mid-to far infrared absorption and reflectivity measurements
in the neighborhood of the strong reststrahlen absorption
bands of most semiconductors (20 to 70 μm wavelength). It was
employed in the reststrahlen and local mode (impurity) absorption
measurements in CdS, CdSe and α - HgS and in doped and undoped
ZnSe laser window specimens. The infrared spectrometer has a
1.5 meter focal length (f/7 optics) and is capable of $1 cm^{-1}$
resolution in the far infrared and approximately $0.5 cm^{-1}$ in
the near infrared. It also employs several different types of
infrared detectors, including diamond window Golay cells, as
well as fast photoconductive and helium-cooled semiconductor
bolometer detectors for selected spectral ranges. Housed in
a large vacuum tank, this spectrometer was designed so that it
could be used in conjunction with cryogenic optical Dewars, as
well as superconductive magnet Dewars.

3. ENERGY BAND STRUCTURE

We shall be concerned here primarily with those II - VI
and III - V compound semiconductors which crystallize in either
the wurtzite hexagonal, or the zincblende cubic structures.
At this point in time, the energy band structure throughout
the Brillouin zone, and particularly at the high symmetry points,
is very well understood in nearly all of the II - VI and
III - V semiconductors which crystallize in these structures.
Much of this understanding has come from the enormous number
of theoretical energy band calculations which have been performed
over the past few years, such as those performed by the ARL
Solid State Theory Group, using various plane wave methods,
as well as those performed by other groups, using several
different theoretical approaches (See T. C. Collins, ARL Final
Report No. TR 75-0020, February 1975, and the references cited
therein). And there is little doubt that the experimental
optical data obtained from semiconductor spectra have contributed
considerably to the success of these theoretical energy band
studies.

14

As noted in Section II, CdS, CdSe, ZnS and ZnO readily crystallize in the wurtzite structure, and, for our purposes here, we shall be concerned mainly with the wurtzite energy band structure at the center of the Brillouin Zone (Γ - symmetry point, near $\underline{K} = 0$). This point in $\underline{K}$-space defines the forbidden energy gap at the conduction and valence band extrema; it is also the E vs $\underline{K}$ region which is appropriate to our studies of exciton structure, bandgap transitions and impurity states.

At $\underline{K} = 0$, the wurtzite band structure is characterized by a conduction band minimum of Γ_7 symmetry. It is also characterized by a six-fold degenerate valence band maximum of Γ_{15} symmetry, in the absence of spin-orbit and crystal field interactions; in the presence of these perturbations, the Γ_{15} valence band splits into three two-fold degenerate bands of the following symmetries; a top valence band (A-band) of Γ_9 symmetry and two lower split-off bands (B- and C-bands), each of Γ_7 symmetry. It is interesting to note that the Γ_{15} valence band is equivalent to that of the zincblende structure in the absence of spin-orbit interaction. The splitting of the wurtzite valence band arises from a mixed spin-orbit and crystal field interaction. The separations of these three valence bands are defined by the relations

$$E_{AB} = (\Delta_{So} + \Delta_{Cr})/2 - [(\Delta_{So} + \Delta_{Cr})^2/4 - 2\Delta_{So}\Delta_{Cr}/3]^{\frac{1}{2}},$$

$$E_{BC} = (\Delta_{So} + \Delta_{Cr})/2 + [(\Delta_{So} + \Delta_{Cr})^2/4 - 2\Delta_{So}\Delta_{Cr}/3]^{\frac{1}{2}}, \quad (1)$$

from which approximate values of the spin-orbit and crystal field energies, Δ_{So} and Δ_{Cr}, may be calculated. For all practical purposes, the wurtzite structured materials are direct bandgap semiconductors and have direct allowed optical transitions. In terms of atomic orbitals, the conduction band states are predominantly S-like in character and the valence band states are predominantly p-like. Optical transitions between the valence and conduction bands obey polarization selection rules which have been determined from group theory. For example, a $\Gamma_7 - \Gamma_9$ transition is allowed only for $\underline{E} \perp C$, where C is the crystalline c-axis of the wurtzite lattice and $\underline{E}$ is the electric vector of the radiation. A $\Gamma_7 - \Gamma_7$ transition, on the other hand, is allowed for both modes of polarization ($\underline{E} \parallel C$ and $\underline{E} \perp C$). It is this property of the wurtzite band structure which gives

rise to the absorption dichroism commonly observed in CdS, CdSe, ZnS and ZnO. Since free excitons are hydrogenically-bound electron-hole pairs, whose electrons and holes derive from the conduction and valence bands, respectively, one would expect the exciton symmetry to depend upon the symmetry of the bands to which it belongs and it does. However, the total symmetries (irreducible representations) of the exciton states are defined by a product representation of the conduction and valence band symmetries and the exciton symmetry. This gives rise to exciton states whose symmetries and optical selection rules are different from those of the conduction and valence bands. Similar arguments can also be made for the symmetries and selection rules of exciton complexes (impurity excitons). Optical selection rules are often extremely useful in identifying the optical transitions in semiconductor spectra and have frequently been used for this purpose in the present work. These points will be discussed further in Section III-6 (Exciton Structure).

Zincblende is the other crystal structure which shall be of interest to us here. Virtually all of the III-V compounds and many of the II-VI compounds normally crystallize in this relatively simple cubic structure. The zincblende energy band structure is relatively simple at the Γ-symmetry point. At $\underline{K} = 0$, it is characterized by a conduction band minimum of $\overline{\Gamma}_6$ symmetry. As noted above, it is also characterized by a valence band maximum of Γ_{15} symmetry, in the absence of spin-orbit interaction. In the presence of spin-orbit interaction, the valence band splits into two bands: a top valence band of Γ_8 symmetry and lower split-off band of Γ_7 symmetry. In materials of this structure, optical transitions between conduction and valence bands are unpolarized. Moreover, excitons formed from the conduction and valence bands of the zincblende structure have states whose symmetries differ from those of the wurtzite lattice. All of the zincblende semiconductors which have been considered in the present report are characterized by direct bandgaps.

The experimental values of the zone center separations (Γ-point) of the conduction and valence band edges in the II-VI compounds are given in Table I. These precise values of bandgap and valence band separations have been determined mostly from intrinsic exciton spectra, in which the hydrogenic exciton effective mass approximation was assumed. Exciton spectra will be discussed in Section III-6.

4. INTRINSIC SPECTRAL CHARACTERISTICS OF SEMICONDUCTORS

a. Optical Dispersion

In electrical terms, there are two extremes in which material media may be classified: 1) dielectric insulators and 2) metallic conductors. Although semiconductors belong to neither extreme, it has long been recognized that their electrical and optical properties have much in common with those of the two extremes. For example, semiconductors transmit, absorb and disperse optical radiation just as insulators do, and, at the same time, they also conduct electrical charge and have relatively high conductivities. As their name suggests, semiconductors are part-insulator and part-conductor and they are characterized by both dielectric and metallic properties. In our treatment of the intrinsic spectral characteristics of semiconductors, it is of interest to consider the simple classical theory of optical dispersion in dielectric media. The optical constants and dispersion relations which can be derived from classical dielectric theory are also applicable to semiconductor media and offer at least a semi-quantitative description of the dispersion and absorption which arises from the motion of both bound and free electrons, produced by the incident electromagnetic radiation field. Free excitons also produce dispersion and their spectral characteristics definitely belong to the intrinsic spectral characteristics of the semiconductor in which they are formed. In fact, it is now generally recognized that the low temperature bandgaps of most II-VI and III-V semiconductors can be determined much more precisely from the analysis of exciton spectra than from the analysis of broad absorption adge spectra.

The classical disperison treatment of Lorentz considers the pure dielectric as an assembly of oscillators set in forced motion by the incident radiation field. In this model we shall be concerned with the polarization arising from the displacement of bound electrons from their equilibrium positions, the displacement being produced by the periodic field of the incident radiation. The equation of motion of such electron can be written as

$$m^* \ddot{x} + m^* \gamma \dot{x} + m^* \omega_o^2 x = eEe^{i\omega}, \qquad (2)$$

where m^*, e and x are, respectively, the effective mass, charge and displacement of the electron, $m^* \omega_o^2 x$ is the restoring force, $m^* \dot{x}$ is the damping force, $Ee^{i\omega t}$ is the applied periodic field, ω is a characteristic frequency and γ is a damping factor given by $\gamma = 1/T$, where T is the collision time.

The solution of this equation varies sinusoidally and its complex amplitude is given by

$$x = (eE/m^*)/(\omega_o^2 - \omega^2 + i\omega) \qquad (3)$$

from which we may calculate the oscillating dipole moment, ex, and the polarization, P, of the medium in which there are N electrons per unit volume

$$P = Nex/E. \qquad (4)$$

In dielectrics of non-vanishing conductivity, the refractive index is complex and may be written as

$$N = (n - ik) \qquad (5)$$

where n is the real part of the index, and k is the absorption index which is proportional to the conductivity, $2nk\omega\varepsilon_o$. For the same reason, the dielectric function of the medium is also complex and may be expressed as

$$\varepsilon_c = (n-ik)^2 = (n^2 k^2 - i2nk), \qquad (6)$$

Since $\varepsilon = N^2$. Both N and ε_c depend on the frequency or wavelength, since n and k are frequency-dependent. The complex dielectric function is related to the polarization by

$$\varepsilon_c = 1 + P/\varepsilon_o, \qquad (7)$$

where ε_o is the dielectric permativity of free space. Combining Equations (6) and (7) and substituting Equations (3) and (4), we obtain

$$(n-ik)^2 = 1 + (Ne^1/m^*\varepsilon_o)/(\omega_o^2 - \omega^2 + i\omega), \qquad (8)$$

Equating real and imaginary parts of Equation (3), we obtain

$$n^2 - k^2 = 1 + (Ne^2/m^*\varepsilon_o) \times \frac{\omega_o^2 - \omega^2}{(\omega_o^2 - \omega^2)^2 + \omega^{2 2}} \qquad (9)$$

and

$$2nk = (Ne^2/m^*\varepsilon_o) \times \frac{\omega}{(\omega_o^2 - \omega^2)^2 + \omega^{2 2}} \qquad (10)$$

Equations (9) and (10) are the classical dispersion relations which relate the optical constants, n and k, to the radiation frequency, ω, in a dielectric medium. As noted above, n and k are not actually constants; they are slowly varying functions of the

frequency, ω, except in regions of intrinsic absorption where they vary rapidly with frequency. These classical dispersion relations provide approximate descriptions of the dispersion and absorption which arises from the motion of bound electrons in semiconductors. The left-hand side of Equation (9), $n^2 - k^2$, is the real part of the complex dielectric function, ϵ_c, while the left-hand side of Equation (10) is its imaginary part, as we can see from Equation (6). We note from Equation (10) that 2nk rises through a maximum as $\omega \to \omega_o$, which corresponds to an absorption band centered at ω_o, such as the broad absorption peak (continuum) which arises from the band-to-band transitions at the bandgap and which commences at the absorption edge of the semiconductor, Equation (1) represents a single oscillator and thus has only one maximum in 2nk (at $\omega = \omega_o$). For wavelengths much longer than those in the absorption band centered at $\omega = \omega_o$, k becomes negligible in comparison to n, and Equation (9) may be approximated by

$$n^2 - 1 = (Ne^2/m^*\epsilon_o)/(\omega_o^2 - \omega^2). \qquad (11)$$

As $\omega \to o$, Equation (10) shows that the absorption is small and Equation (11) reduces to

$$n_o^2 - 1 = Ne^2/m^*\epsilon_o \, \omega_o^2, \qquad (12)$$

which has been used to calculate accurate values of the long wavelength limit of the refractive index in several semiconductor materials. In polar semiconductors, such as the II-VI and III-V compounds, there are actually two very strong absorption bands which characterize the intrinsic absorption spectrum: one which occurs at the absorption edge (bandgap) and another (the lattice absorption band) which occurs in the longwave (infrared) region. The simple, single-oscillator, classical model of dielectric dispersion does not account for the two absorption bands simultaneously, nor does it account for other weaker optical transitions (electronic and lattice mode) which characterize the semiconductor and which alter the dispersion relations and hence the absorption spectrum. Nevertheless, the simple oscillator model provides some useful insights regarding the physics of optical dispersion produced by the polarization of moving charges in a semiconductor medium.

The more exact quantum mechanical treatment of dispersion considers the interaction of the radiation field with atomic and molecular states, and yields expressions which are very similar to the classical result, except that they contain a sum of terms like those on the right-hand side of Equations (9) and (10). These terms represent a set of linear oscillators each of which has a resonance frequency corresponding to allowed transition. Thus, in the quantum mechanical result, Equation (10) becomes

$$2nk = \sum_i \frac{(Ne^2 f_i/m^*\epsilon_o)\,(\omega_i^2 - \omega^2)}{(\omega_i^2 - \omega^2)^2 + \omega^2\gamma_i^2} \qquad (13)$$

19

The magnitude of the contribution of each oscillator to the optical constants is determined by the oscillator strength f_i of each transition.

If 2nk, the imaginary part of the dielectric function, is known as a function of ω over a wide range of frequency, for all of the quantized oscillators which contribute to the absorption processes in a given semiconductor material (electronic band-to-band transitions plus lattice mode contributions), then we may plot a curve of 2nk vs. ω, the peaks of which correspond to absorption maxima in the spectrum of the material. The absorption of a dielectric medium is always determined by the imaginary part of its frequency-dependent dielectric function. β, the absorption coefficient of an optically transparent medium, is defined by the condition that the energy in the incident wave fall to $1/e$ of its initial value in a distance $1/\beta$, and is given by

$$\beta = 2\omega k/c = 4\pi k/\lambda. \tag{14}$$

β is commonly expressed in units of cm^{1}. If n is known as a function of frequency, we can, in principle, calculate k as a function of frequency from Equation (13) and hence, from Equation (14), the absorption coefficient as a function of frequency which corresponds to the absorption spectrum of the semiconductor. From energy band calculations performed in ARL's Solid State Theory Group, the excitation energies and the imaginary parts of the dielectric functions have been determined for a number of II-VI and III-V semiconductors and the calculated absorption has been in very good agreement with the optically measured values.

We turn now to a consideration of the optical transmission and reflection properties of semiconductors. Their spectral transmission characteristics make semiconductor materials very useful for many optical applications, such as windows, lenses and band-pass filters of varying refractive index, dispersion and reflectivity. In the broad spectral region between the reststrahlen absorption band, semiconductors are characterized by a relatively high optical transmission, and the same is also true of highly ionic dielectric materials. We have made use of this property in our studies of high power infrared laser windows materials, in which we have measured and studied the transmission properties of CdTc, CdSe and ZuSe at a wavelength of 10.6μm, radiated by high power CO_2 lasers. When grown to high crystal quality and low impurity concentrations, these materials have very good spectral transmission at wavelengths between their band-gaps and about 30μm, where the lattice absorption bands begin, and are characterized by extremely low absorption coefficients at 10.6μm, as indicated in Section V.

In the absence of Fresnel reflection losses, the attenuation of optical transmission through material media can be

20

expressed in terms of the definition of absorption coefficient given in Equation (14). The attenuation is given by

$$I/I_o = \exp(-\beta d),\tag{15}$$

where I is the transmitted and I_o the incident intensity or power, β is the absorption coefficient, d is the thickness of the material, and it is understood that I/I_o is the attenuation at a particular frequency, since β varies with frequency. However, the transmission of electromagnetic radiation through dielectric materials always suffers reflection losses at the interfaces, and these losses are determined by the refractive index and the conductivity of the material. For electromagnetic waves reflected from a dielectric, we may write

$$r + R^{\frac{1}{2}} e^{-i\phi} = R^{\frac{1}{2}} \quad (\cos\phi - i\,\sin\phi)\tag{16}$$

for the complex amplitude of reflection at the surface, where R is the power reflection coefficient, or reflectivity, and ϕ is the phase angle. At normal incidence (in air), the complex amplitude of reflection at the interface of a dielectric is given by

$$r = \left| \frac{N-1}{N+1} \right|\tag{17}$$

which, on substituting the complex refractive index from Equation (5), becomes

$$r = \left| \frac{n-i\,k-1}{n-i\,k+1} \right|\tag{18}$$

and, since the reflected intensity (reflectivity) is given by the square of the amplitude, we may further write

$$R = \left| \frac{n-i\,k-1}{n-i\,k+1} \right|^2,\tag{19}$$

which, when rationalized, becomes

$$R = \left| \frac{(n-1)^2 + k^2}{(n+1)^2 + k^2} \right|.\tag{20}$$

For pure dielectrices and most wide bandgap semiconductors, we may assume that k makes a negligible contribution to the reflectivity in a spectral region of high transmission. Hence we may rewrite Equation (20) as

$$R = \left| \frac{n-1}{n+1} \right|^2.\tag{21}$$

21

Equations (19) and (20) relate the optical constants n and k to the reflectivity, R, which can be determined from spectral reflectivity measurements. The reflectivity varies as a function of frequency and R (ω) will rise abruptly through a maximum and then fall through a minimum in the neighborhood of an absorption band. If R is known as function of frequency (from spectral measurements), then n and k and hence 2nk can be calculated as a function of frequency. And, of course, from 2nk vs. ω, the absorption spectrum of the semiconductor can be determined. Semiconductor reflection spectra have often been used in the present work to determine the positions (frequencies) of absorption bands in highly absorbing spectral regions where the transmission was almost totally attenuated, at the absorption edge, e.g., and this will be discussed further in Section III-4b, below. Equation (21) can be used to calculate the nearly constant background reflectivity in a region of high transmission, if n is known from an independent measurement. R can also be determined directly from spectral reflectivity measurements. This has been done for a number of the II-VI compounds in the present work and there is good agreement between calculated and experimental values of R, when proper account is taken of the rapidly attenuated, multiple internal reflections which occur in dielectric layers. It is usually sufficient to consider only two reflections in the calculated values.

A useful expression for the optical transmission of absorbing media can be derived from dielectric multi-layer theory. Consider a plane-parallel dielectric plate of thickness d. In the absence of interference fringes, it is easy to show that the average, normal-incidence transmission of this plate is given by

$$\text{Tav.} (\omega) = \frac{(1-R)^2 \exp\left[-\beta(\omega)d\right]}{1-R^2 \exp\left[-2\beta(\omega) d\right]} \tag{22}$$

In a region of high transmission, R is usually small and does not vary much with frequency, particularly in the highly ionic dielectrics and in wide bandgap semiconductors. Hence we may assume that

$$\exp (2\beta d) \gg R^2,$$

even when β and d are relatively small. In this approximation, we may rewrite Equation (22) as

$$\text{Tav.} (\omega) = (1-R)^2 \exp\left[-\beta(\omega)d\right] \tag{23}$$

From their experimentally measured transmission spectra, semiconductor absorption coefficients can be calculated as a function of frequency from Equations (22) or (23). While Equation (22) provides reasonably accurate values of absorption coefficients at moderate absorption levels, it can not be used to calculate absorption coefficients when the absorption losses are extremely small, owing to the difficulty in making accurate transmission

measurements at extremely low absorption levels. In the case of the infrared laser window specimens, for example, their low absorption coefficients were measured calorimetrically. This was achieved by pulsing the specimens with a laser beam of known frequency and power and then measuring the small temperature rise in the specimen due to the heat absorbed from the beam. From the temperature rise and the measured power of the laser pulse, together with known values of the specimen's mass, length and refractive index, it was possible to calculate the absorption coefficients of laser window specimens, which fall in the range of 0.001 cm^{-1} and below.

The dispersion of free carriers also contributes to the background absorption of semiconductors. Metallic or free carrier absorption arises from the motion of free electrons (or holes) in the semiconducting medium. Of course, perfectly free electrons moving in the perfectly periodic field of a crystal lattice do not absorb radiation. Free carrier absorption arises from the fact that there is scattering of the carriers as they move in the energy bands of the lattice. And there are several mechanisms by means of which the charge carriers can be scattered in polar semiconductors, such as ionized impurity, acoustic mode, polar mode and piezoelectric scattering. As in the case of bound electrons (Equation (2)), the dispersion of free electrons can also be treated classically. Equation (2) becomes the equation of motion for free electrons when we set the restoring force, $m^*\omega_o^2 x$, equal to zero. Thus, for the case of free electrons, the dispersion relations of Equations (9) and (10) become

$$n^2 - k^2 = 1 - (Ne^2/m^*\varepsilon_o)/(\omega^2 + \gamma^2) \tag{24}$$

and

$$2nk\omega = (\gamma Ne^2/m^*\varepsilon_o)/(\omega^2 + \gamma^2), \tag{25}$$

since $\omega_o = 0$. At small absorption ($n^2 >> k^2$) and at frequencies high compared to the collision frequency ($\omega^2 >> \gamma^2$), Equation (24) reduces to

$$n^2 = 1 - Ne^2/m^*\varepsilon_o\omega^2. \tag{26}$$

From the definition of absorption coefficient given in Equation (14), we can then write

$$\beta = \frac{2\omega k}{c} = \gamma \ Ne^2/m^*\omega^2\varepsilon_o \ nc \tag{27}$$

Changing from frequency to wavelength and putting Equation (27) in terms of the carrier mobility ($\gamma = 1/\tau; \ \tau = \mu m^*/e$), we obtain

$$\beta = \frac{\lambda^2 e^3}{4\pi^2 c^3 n\varepsilon_o} \left[\frac{N}{m^*\mu} \right], \tag{28}$$

23

which is equivalent to the classical Drude expression for the free carrier absorption of a single type of carrier. Equation (28) shows that the free carrier absorption increases with increasing carrier concentration; it also increases with the square of the wavelength and becomes strong in the longwave infrared region. In fact, at high carrier concentrations, the far-infrared free carrier absorption can become strong enough to block the transmission of very thin semiconductor specimens. This is particularly true of the narrow bandgap materials. In infrared laser window materials, free carrier absorption can be a problem if the carrier concentration is not extremely low at room temperature.

Experimental values of the II-VI compound dielectric data are presented in Table II. The static dielectric constants, ε_s, have been determined mostly by Berlincourt and coworkers and were calculated from the experimentally measured values of the elastic constants. They have also been measured electrically. The high frequency dielectric constants have been determined mostly from experimentally measured values of the refractive index ($\varepsilon_\infty = n^2$). Most of the refractive indices have been measured either refractively or interferometrically in single crystal specimens.

b. Absorption and Reflection at the Bandgap

Although the simple disperison model provides a conceptually useful picture of the disperison and absorption processes in semi-conducting dielectrics, we cannot expect the single bound oscillator to predict the detailed spectral features of intrinsic absorption in real semiconductors. In practice, we must invoke the energy band model whose quantized energy bands (and States) are the property of the periodic crystalline lattice. We must then consider the many allowed optical transitions which occur between these energy bands, in order to accurately describe the dispersion and absorption of quantized radiation in the semiconductor. And, of course, these quantized optical transitions are determined by the energy band symmetries, as well as momentum and polarization selection rules. The spectral absorption edge is one of the most unique and striking features of semiconductor materials. In each material, it falls at a different spectral position (wavelength) and provides not only a measurement of the separation of conduction and valence band edges (and hence the bandgap), but also a means of classifying and predicting many of the optical, thermal and electrical transport properties of semiconductors. Absorption and reflection measurements of the optical transitions in the spectral region of the bandgap yield a wealth of information regarding the intrinsic energy band structure, particularly the intrinsic exciton structure, since it is in this spectral region that the intrinsic exciton transitions are observed. The optical transitions of shallow donor and acceptor impurities also fall in this spectral region and much can be learned about impurities and defects from

24

such spectral measurements, particularly when performed as a function temperature and in the presence of perturbing electric and magnetic fields.

In many of the wide bandgap II-VI compounds, which crystallize in the zincblende structure, such as ZnSe, ZnTe and CdTe, the conduction and valence bands are simple and parabolic near the center of the zone (near $\underline{k} = 0$). In this approximation, we may write for the conduction and valence band energies

$$E_c = E_G + \frac{{}^2k^2}{2m_e^*} \quad \text{and} \quad E_v = - \frac{{}^2k^2}{2m_h^*}$$

which yield

$$\omega = E_c - E_v = E_G + \frac{k^2}{2\mu} \tag{29}$$

for the energy of the optical transition between conduction and valency band states. Solving the interaction Hamiltonian for the Bloch wave states in these bands, we obtain an expression for the absorption in terms of the momentum matrix element of the interaction, $\underline{P}cv$, and the joint density of states of the bands, which when substituted in Eqaution (29) yields an expression for the absorption coefficient of the interband transitions

$$\beta = \frac{4_{\P}{}^2 e^2}{nm^2 c(\omega)} \quad (2\mu)^{3/2} (\omega - E_G)^{\frac{1}{2}} / 2_{\P}{}^2{}^3 \quad \underline{a} \cdot \underline{P}cv^2 \tag{30}$$

where

    ω is the photon energy of the transition
    n is the refractive index
    $\underline{a}$ is the polarization unit vector and
    $\mu = m_e^* m_n^* / (m_e^* + m_n^*)$.

For transitions allowed to first order, the momentum matrix element $\underline{P}cv$ is a slowly varying function of energy. Equation (30) is strictly valid over a small range of $\underline{k}$, near $\underline{k} = 0$ ($\omega \sim E_G$). When β is plotted as a function of $(\omega - E_G)/E_G$, the absorption rises very steeply and saturates into the continuum of band states, thus defining the absorption edge of the semiconductor. The quantum mechanical model provides a more accurate description of the shape of the absorption edge than does the classical oscillator. Spectral measurements have been made of the absorption edge over a wide range of temperatures in most of the II-VI compounds in order to optically characterize the band parameters in these materials.

As the photon energy, ω, rises above the bandgap, there is a rapid attenuation of the transmission given by Equation (22) due to the strong continuum absorption of the quantum states in the valence and conduction bands. In order to study the optical

transitions between these higher conduction and valence band states, it is necessary to employ reflection spectroscopy. This technique also provides details of the exciton spectra not observed in absorption (transmission) spectra. In analyzing the reflectivity, $R(\omega)$, we find that there are anomalies in the reflection spectrum (maxima and minima) which correspond to the frequencies of optical transitions in the semiconductor. These anomalies are produced by the dispersion of the optical constants. Through various spectral weighting techniques, such as Kramers-Kronig analysis, it is possible to calculate values of the absorption coefficient for specific optical transitions from quantitative spectral measurements of the reflectivity. This is possible because of the analytical relation which exists between the reflectivity, $R(\omega)$, and the optical constants, $n(\omega)$ and $k(\omega)$, defined for example, for the bound oscillator in Equations (9) and (10), and is done in the following way: the phase angle between the incident and reflected radiation waves is related to the reflectivity and defined by Equation (16); it is also related to the reflectivity by one of the Kramers-Kronig relations

$$\phi(\omega p) = \frac{\omega p}{\Pi} \int_{o}^{\infty} \frac{\log R(\omega p)/\log R(\omega) \, d\omega}{\omega^2 - \omega p^2} \tag{31}$$

where ωp is a given frequency point on the reflectivity curve, over which the integral is to be evaluated from $w = o$ to $w \to \infty$. Equating real and imaginary parts of Equations (16) and (18), we obtain expressions for the optical constants, n and k, in terms of $R(\omega)$ and $\phi(\omega)$,

$$k(\omega) = \frac{2R^{1/2} \sin \phi}{1 + R - 2R^{1/2} \cos\phi} \tag{32}$$

$$n(\omega) = \frac{1 - R}{1 + R - 2R^{1/2} \cos\phi} \tag{33}$$

Equation (31) is summed numerically to obtain values of $\phi(\omega p)$ at each frequency point of the experimentally measured reflectivity, $R(\omega)$. From Equations (32) and (33) and the known values of $R(\omega)$ and $\phi(\omega)$, we can calculate the imaginary part of the dielectric function (2nk) as a function of frequency (ω). From Equation (14), and the known values of n and k, we can also calculate the absorption coefficient (β) as a function of frequency (ω). In this way the absorption spectrum of the semiconductor can be calculated from its reflection spectrum, and hence the resonant frequencies (energies) of the optical absorption transitions. In the present work, this technique was employed to analyze the vacuum ultraviolet reflection spectra of II-VI semiconductors in order to determine the transition energies between the higher conduction and valence bands, such as those at the Γ, X, L and M symmetry point in ZnO and CdSe wurtzite structures.

26

c. Reststrahlen Absorption

The spectral transmission of semiconducting dielectric materials is bounded in the short wavelength region by the bandgap (ultraviolet to near infrared) and in the long wavelength region by the broad reststrahlen absorption bands, which range from about 25 µm in ZnO, out to 70 µm in CdTe. The longwave absorption bands arise from the lattice vibrations, mainly the optical modes. Only the transverse optical modes are infrared allowed in the symmetries of the zinc blends and wurtzite II-VI compounds. The longitudinal optical modes are not observed in infrared absorption, but, knowing the static and high frequency dielectric constants, ε_s and ε_∞, they can be calculated from the relation

$$\frac{\omega_{TO}}{LO} = \left(\frac{\varepsilon_\infty}{\varepsilon_s} \right)^{\frac{1}{2}}. \tag{34}$$

The strong TO mode absorption band is very broad, even at low temperature, where the optical mode lattice vibration bands sharpen markedly and most of the acoustic mode structure disappears. Consequently, it is difficult to determine the center frequency of the broad TO phonon band from infrared absorption spectra. In practice, the lattice vibrational absorption bands are determined from infrared reflection spectra, in which the absorptions give rise to relatively sharp maxima and minima. The absorption frequencies are then determined by Kramers-Kronig analysis, as described above, or by fitting a classical oscillator to the reflectivity spectrum. Combination bands of the optical and acoustic vibrational modes, such as 2TO, LO + To, LO + TA, and TO + LA, are also observed in the infrared reflection and absorption spectra. The characteristic LO and TO phonon frequencies of the II-VI compounds, mostly determined from infrared spectral measurements, are presented in Table III.

In recent years, Raman scattering of laser light from phonon states has been increasingly employed as a technique for the study and measurements of phonon dispersion in semiconductors. In stokes scattering, the incident laser photons lose an energy equal to that of the phonons through preferential, in elastic scattering from phonon states. Spectral analysis of the Raman scattered radiation reveals sharp peaks at photon energies below that of the pump laser, and their spectral separations from the laser peak correspond to the phonon energies. Not all of the phonon modes are Raman active, but the frequencies of those which are observed can be determined very precisely. Raman spectroscopy has been employed in the present work to study the phonon frequencies of CdTe and CdS.

A novel technique, which makes use of the large electron-phonon coupling to impurity states in polar semiconductors, has also been employed in the study of phonon dispersion in CdS and ZnO. In this technique, the experimental data are obtained from photoluminescence spectroscopy of bound exciton eomplexes, which will be discussed further in Sections III-5 and III-6. Because

27

of the electron-phonon coupling, the bound exciton emission lines
are accompanied by a series of sharp phonon-assisted emission
lines (phonon replicas) which arise from coupling to the optical
mode phonon states (mostly LO modes). These sharp lines, which
are equally spaced and separated by the phonon energy, provide
accurate experimental values of the phonon frequencies. Using
the experimental phonon frequencies, in conjunction with a mixed-
bonding lattice band model, the dispersion curves for the phonon
states of CdS and ZnO have been calculated for all of the principal
zone-center and zone-boundary symmetry points (Γ, A, and K).
These dispersion curves provide accurate values of the phonon
frequencies in these two materials, a few of which are presented
in Table IV.

5. IMPURITY SPECTROSCOPY

a. Photoluminescence Spectra

Photoluminescence is the optically-excited radiation which is
emitted by crystalline solids. In semiconductors, it is largely
an extrinsic phenomenon, since most of the emitted radiation
arises from the radiative recombination of charge carriers (holes
or electrons) bound to impurities and defects (donors and acceptors),
and falls at photon energies below the intrinsic absorption edge
defined by the bandgap, which is the extrinsic spectral region.
The recombination radiation which is observed in the extrinsic
spectral region can arise from free-to-bound, as well as bound-to-
bound, optical transitions. There are several possibilities of
extrinsic recombination: 1) free electrons with bound holes;
2) free holes with bound electrons; 3) bound electrons with bound
holes; and 4) the recombination of bound exciton complexes. The
recombination of intrinsic carriers (free holes and electrons)
is also possible, but the capture cross-sections and hence the
transition probabilities for such processes are very small;
similarly, the recombination of free excitons is also possible and
has been observed, but the recombination radiation is very weak.
Consequently, these intrinsic processes contribute very little to
the total intensity of an extrinsic photoluminescence spectrum.
In the II-VI compounds, most of the extrinsic photoluminescence
is observed in a narrow spectral region close to the intrinsic
absorption edge and is called edge-emission. In this report, we
have used the terms photoluminescence, edge-emission and emission
synonymously. Spectral analysis reveals that the edge-emission
comprises a sharp series of emission lines very close to the
absorption edge and a series of broader, phonon-assisted emission
peaks at somewhat lower energies.

Intense photoluminescence is observed in many polar semi-conductors at low temperatures. When spectrally analyzed, this intense photoluminescence provides a rich source of experimental data concerning the electronic states of impurities and defects in such semiconductors, particularly in the II-VI compounds, such as CdS, CdSe, CdTe, ZnO and ZnS, where the intrinsic band structure and the exciton properties are now well understood. The many sharp lines which appear in such spectra, particularly those of bound excitons, provide a "finger print" of the impurities and defects which are present in the semiconductor lattice.

In the early work of this task, the research effort was concentrated on spectral characterization studies of the photo-luminescence and on identifying the trapping centers which gave rise to the broad emission, from which a consistent edge-emission-model was established for CdS; later, the effort shifted to intensive studies of the sharp-line emission, aimed at identifying the bound exciton impurity transitions and at achieving a better understanding of the residual impurity and defect structure in the II-VI compounds. From studies of the sharp spectral emission lines and their magnetic-field-splittings, it is possible to differentiate between neutral and ionized donor and acceptor impurities. In conjunction with systematic impurity doping experiments, specific donor and acceptor impurities have been identified from the spectra of CdS and CdSe platelet crystals. The magneto-optics of bound-exciton impurities (complexes) will be discussed further in Section IV.

One of the most striking features in the photoluminescence spectra of the II-VI compounds is the phonon-assisted edge-emission, which appears as a series of equally-spaced emission peaks, separated by the LO phonon energy, whose intensities fall with increasing wavelength. As many as seven of these peaks are absorbed in CdS. The phonon-assisted emission is very intense in the highly polar II-VI compounds, such as CdS, ZnO, ZnS and ZnSe, and arises from the coupling of the electronic impurity states to the phonon states of the lattice. Most of the II-VI compounds have a large electron-phonon (polaron) coupling constant. In these materials, phonon-assisted transitions are observed from the radiative recombination of bound impurities and from the radiative collapse of bound exciton complexes. The phonon-assisted emission lines arising from the latter are very sharp and narrow and their separations provide an accurate measurement of the optical mode phonon frequencies which are in good agreement with those determined by other methods. The phonon frequencies of CdS and ZnO have been measured from such spectra and are much more precise than the values determined from infrared re-flectivity measurements at the reststrahlen absorption band.

As noted above, the recombination of free excitons is also possible. Such recombination radiation has been observed in the extrinsic photoluminescence spectra of high-equality CdS platelets, including transitions from the ground and excited configurations of the free exciton. From these spectral data, the intrinsic exciton structure of CdS has been very precisely determined.

b. Pair Spectra

Not all of the sharp-line emission observed in the photoluminescence spectra of CdS arises from the radiative recombination of bound exciton complexes. Many of these sharp lines, which appear between the broad-green, phono-assisted emission peaks and the absorption edge, have been identified as the recombination radiation of donor acceptor pairs. As noted above, the broad-green, phonon-assisted peaks arise from the recombination of free and bound carriers at simple bound impurity centers. In the Reynolds edge-emission-model, there are two principal series of broad phonon-assisted peaks, one beginning at 5130Å (recombination of free electrons with the trapped holes of the acceptor center). Actually, there is another series of broad emission peaks, beginning at 5163Å, which is associated with the 5179Å series, and which is also interpreted as bound-to-bound recombination radiation. The donor acceptor pair emission lines arise from the bound-to-bound recombination of preferential pairs of donor and acceptor centers which are located on widely separated lattice sites. For example, first and second nearest neighbor pairs, as well as other distant pairs can exist, and the recombination for each discrete separation gives rise to emission at a discrete photon energy. The photon energies of the pair lines are, in general, given by

$$E = Egap - (E_D + E_A) - e^2/\varepsilon_s r, \tag{35}$$

where Egap is the bandgap energy, E_D and E_A are the donor and acceptor binding energies, and r is the separation of the donor and acceptor centers of each pair. The donor-acceptor pair lines appear as a series of sharp spectral lines which can verge in the limit $(r \rightarrow 0)$ to the broad-green, phonon-assisted bands in CdS, as indicated in the above expression. In the present work, a CdS donor-acceptor pair series which converges to the 5163Å series of broad-green, phonon-assisted peaks has been identified. Other donor-acceptor pair spectra have been observed in GaP and CdS by the Bell Telephone Laboratory group.

c. Far Infrared Impurity Absorption

We have indicated above how bandgap photoluminescence and absorption spectroscopy has been employed in the analysis of defects

and impurities in the II-VI compounds. As noted in the Introduction (Section I), far infrared absorption spectroscopy offers an alternative technique for the detection and study of foreign impurities and defects in semiconductors. Most of the shallow donor and acceptor activation energies in the II-VI and III-V semiconductors lie in an energy range between about 50 and 3meV (400 to 24 cm^{-1}), which corresponds to an infrared wavelength range of approximately 25 to 500 μm. These wavelengths are easily within the operating range of conventional Fourier Transform Spectrometers (Michaelson Interferometric Spectrometers). Fourier transform absorption spectroscopy has been employed in the present research effort to study the shallow hydrogenic donor transitions in high mobility CdTe and InAs specimens at cryogenic temperatures. The 1S $\rightarrow$ 2P and 15 $\rightarrow$ 3P hydrogenic impurity transitions have been observed and studied in these materials. In the hydrogenic, effective mass approximation, the hydrogenic infrared spectrum of a shallow donor impurity is given by

$$E_I = R(m^*/mo)\ (1/\varepsilon_s^{-2})\ (1/n^2);\ n = 1,\ 2,\ 3.\ .\ . \tag{36}$$

and its binding energy is given by

$$E_{IB} = R^* - R(mo^*/mo)\ 1/\varepsilon_s^2)\ .\ .\ . \tag{37}$$

where R^* is the effective Rydberg, R is the hydrogenic Rydberg (13.6eV), m^* is the electron effective mass (equal to the free electron mass for shallow donors), mo is the rest mass of the electron, and s is the static dielectric constant. In CdTe and InAs, the donor binding energies obtained from fitting the hydrogenic formula to the observed spectra were in good agreement with those calculated from the above expressions and with those obtained by other methods.

6. Exciton Structure

    a. Intrinsic or Free Excitons

    In Section III-4, we have indicated how the bandgap of a semiconductor can be determined from absorption and reflection spectra by directly measuring the spectral position (energy) of the absorption edge, a procedure which usually yields valid results at room temperature. At very low temperatures, however, the bandgap is not precisely defined by such measurements. Under optical excitation at low temperature, intrinsic exciton formation occurs in most semiconductors, and this tends to complicate the absorption spectrum, since the ground and excited states of the exciton lie just below the conduction band edge.

31

Moreover, when excitons are formed, direct (or indirect) optical transitions are not observed between conduction and valence band edges; such transitions occur instead between the valence band maximum and the ground and excited states of the exciton. Hence, the exciton structure must first be determined in order to determine the bandgap energy. The exciton binding energy can be determined from spectral analysis of its hydrogenic ground and excited state transitions. Thus, precise bandgap energies can be determined by adding the exciton binding energy to the experimentally measured photon energy of the ground state transition.

The intrinsic exciton is a hydrogenically bound hole-electron pair, whose hole derived from the valence band and whose electron derives from the conduction band. The intrinsic exciton is also said to be a free quasiparticle, since its hole and electron belong to the valence and conduction band states, respectively; in short, it is a normal mode of the crystal, created by an optical excitation wave, and its wave functions are analogous to those of the block wave states of free electrons and holes. In emission spectra, the free exciton states are observed as the radiative recombination of electron-hole pairs. Both direct and indirect exciton formation occurs in semiconductors, depending on the band structure. The former is characteristic of the II-VI compounds and the latter of Ge and Si. For indirect optical transitions (exciton or band-to-band), momentum is conserved by the emission or absorption of phonons. We will confine our attention here to the simpler direct exciton model which characterizes the II-VI compounds.

In center of mass coordinates, the free exciton wave functions can be written in the form

$$\bar{\Phi}_{\underline{K}, n} = V^{-\frac{1}{2}} e^{-i\underline{k} \cdot \underline{R}} \psi_n(\underline{r}), \ldots \tag{38}$$

where V is the crystal volume, $\underline{K}$ is the exciton center of mass wave vector, and $\underline{R}$ is the center of mass coordinate given by

$$\underline{R} = (m_e^* r_e + m_n^* r_n) / (m_e^* = m_n^*); \ r - r_e + r_h \cdots \tag{39}$$

The plane wave part of this wave function reflects the free-particle motion of the center of mass, while $\psi_n(r)$, the periodic part of the block wave describes the quantum states of the internal motion. $\psi_n(r)$ satisfies the Schrodinger equation

$$[(-h^2/2\mu) \ \nabla_r^2 - e^2/ _s\underline{r}] \ \psi_n(\underline{r}) = E_n \ \psi_n(\underline{r}), \ \ldots \tag{40}$$

where M is the exciton reduced mass given by $\mu = m_e^* m_n / (m_e^* + m_n^*)$. In formulating the exciton Hamiltonian, we have assumed simple spherical energy bands, such as those of the Zincblende cubic

structure near $\underline{K} = 0$. We have also assumed only $\underline{K} = 0$ direct excitons. Except for parametric differences in effective mass and Bohr radius, we recognize the the wave functions, $\psi n(\underline{r})$, are identical to those of atomic hydrogen. The solutions of the Schrodinger equation yield the discrete energy eigenvalues (internal states) of the exciton and are given by

$$E_n = \frac{\mu e^4}{2\hbar^2 \epsilon_s^2} \left(\frac{1}{n^2}\right) ; \quad n=1, 2, 3, \ldots \tag{41}$$

The exciton binding energy is given by

$$E_{ex.B} = \frac{\mu e^4}{2\hbar^2 \epsilon_s^2} = R(\mu/m_o)(1/\epsilon_s^2) = R^*_{ex} \ldots \tag{42}$$

where R^*_{ex} is the effective Rydberg, R is the hydrogenic Rydberg (13.6eV); μ is the effective reduced mass of the exciton, and s is the static dielectric constant. Thus the allowed exciton transitions occur as sharp lines in a hydrogen-like spectrum which coverges to the conduction band continuum. The exciton spectrum is given by

$$E_{ex.n} - E_{gap} - R^*_{ex} (1/n^2) \ldots \tag{43}$$

Usually only the first few lines of the spectrum are observed, since the intensity of the exciton transitions fall off as $1/n^3$. In the case of $\underline{K}+ 0$ excitons (e.g., indirect excitons), an additional term, $\hbar^2 \underline{K}^2 / (m^*_e + m^*_n)$, must be added to the above equation. This term accounts for the $\underline{K}$ - dependent Kinetic energy of the exciton and describes the exciton continuum which is associated with each of the discrete hydrogenic states.

The intrinsic exciton also reflects the anisotropy and symmetry of the valence and conduction bands from which it is formed, as noted in Section III-3. In the Wurtzite-structured II-VI compounds, for example, there is a large anisotropy in valence band effective masses (depending upon which direction is chosen in $\underline{K}$-space, $\underline{K}z$ or $\underline{K}x$, $\underline{K}y$), but the conduction band masses are very nearly isotropic. Thus, when excitons are formed from the bands of the Wurtzite structure, there is an anisotropy in the exciton parameters, due to the anistropic valence band masses and the anisotropic dielectric constant. We can

write the total Hamiltonian for such anisotropic excitons exactly, but the wave equation does not have analytic (closed-form) solutions. However, when certain simplifying assumptions are made, it is possible to obtain approximate solutions to the anisotropic Hamiltonian, which are in very good agreement with experiment, as Thomas and Hopfield have shown for CdS, and as Wheeler and Dimmock have shown for CdSe. In general, a variational approach is used for such calculations, but it is also possible to use perturbation theory when the anisotropy is not too large. In the present work, we have used the approximate theoretical results in our analyses of intrinsic exciton structure in the II-VI compounds, and have obtained very good agreement with the experimental spectra in most cases.

Symmetry also plays an important role in identifying and characterizing the intrinsic exciton transitions. For example, the hydrogenic states of the intrinsic exciton will reflect the symmetrics of the bands form which its hole and electron derive, as noted in Section III-3. In the case of the Wurtzite band structure, the conduction band is of Γ_7 symmetry, while the top valence band (a-band) is of Γ_9 symmetry and the second valence band (B-band) is of Γ_7 symmetry. The irreducible representations (symmetries) of the exciton states are given by the cross-product of the exciton representation and those of the two bands from which the exciton derives. Thus, the irreducible representations of the A-exciton ground state are given by $\Gamma_1 \times \Gamma_9 \times \Gamma_7 = \Gamma_5 + \Gamma_6$. Electric dipole transitions are allowed for exciton states containing Γ_5 symmetry when the radiation is polarized with E⊥C, and are allowed for exciton states containing Γ_1 symmetry when the radiation is polarized with E‖C. From this we note that the A-exciton ground state transition is allowed for E ⊥ c polarization, since the ground state contains the Γ_5 representation. Similarly, the irreducible representations of the B-exciton ground state are given by, $\Gamma_1 \times \Gamma_7 = \Gamma_1 + \Gamma_2 + \Gamma_5$, which shows that the B-exciton ground state transition is allowed for both E‖c and E⊥ c polarizations, since the ground state contains both the Γ_1 and the Γ_5 representations. Thus, we see that the optical polarization selection rules for the ground states of the A- and B-band excitons in the Wurtzite structure are the same as those of the corresponding interband transitions discussed in Section III-3.

The intrinsic exciton properties of the wide bandgap II-VI compounds are now very well understood, after some ten years of extensive research on the optical properties of these materials. Some of the more important intrinsic exciton parameters of the II-VI compounds are summarized in Table V.

6. Bound Excitons

Bound exciton complexes or impurity excitons are also formed in the II-VI compounds and are an extrinsic property of these materials. Bound exciton transitions give rise to sharp spectral lines in the intrinsic spectral region of these materials and are observed in both photoluminescence and absorption. A bound exciton complex is formed by binding a free exciton to a chemical impurity atom (ion) or a host lattice defect. The binding of the exciton to the impurity or defect is relatively weak in comparison to the exciton's binding energy; the resulting complex is molecular-like (analogous to the hydrogen molecule or molecule-ion) and bound excitons have many spectral properties which are analogous to those of simple diatomic molecules. The photon energies of the bound exciton transitions are always slightly below those of the corresponding free exciton transitions, due to the molecular binding. In semiconductors, the chemical centers to which the free excitons are bound can be either neutral donor and acceptor centers, or ionized donor and acceptor centers. Examples of the bound exciton complex model are given below in illustrations (a) and (b):

	upper state	
(a)	lower state	(b)

Exciton Bound to   Exciton Bound to
Neutral Donor   Neutral Acceptor
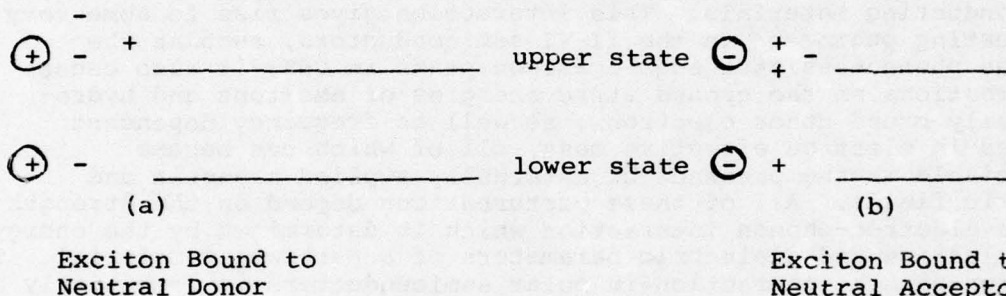
In the upper state of the neutral donor complex (a), the electron spins of the donor and the exciton pair and this state is characterized by the unpaired hole spin; the lower state of this complex is characterized by a single bound electron with unpaired spin. The converse is true for the upper and lower states of the neutral acceptor complex shown in (b). The upper state of (a), for example, is created by optical excitation of free excitons which then bind to the donor center. As the free exciton collapses in a radiative recombination transition, the donor returns to the lower state. Similar models also exist for the case of an exciton bound to an ionized donor and for the case of an exciton bound to an ionized acceptor, except that their upper and lower states will be different from those of (a) and (b), under the perturbing influence of an externally applied magnetic field and when examined as a function of temperature.

The sharp spectral lines of bound exciton complexes are also very strong (large oscillator strength). The strengths of these lines will, in general, depend upon the concentrations of impurities and defects present in the semiconductor lattice, but, in practice, they usually appear stronger in emission spectra then do the intrinsic exciton peaks. They are also very narrow with half-widths at least an order of magnitude less than those of the intrinsic exciton peaks, indicating a relatively long lifetime for the exciton complex state. In magnetic fields, bound complexes also have very unique Zeeman spectral characteristics, from which it is possible to identify the types of electronic impurities to which the free excitons are bound. Bound exciton spectroscopy is, in general, a very powerful analytical tool for the study and identification of impurities and defects in semiconductors, and has been used extensively for this purpose in the present studies of the Wurtzite structured II-VI compounds.

7. Electron-Phonon Interaction

Most of the wide bandgap II-VI compounds are highly polar semiconducting materials. This interaction gives rise to some very interesting phenomena in the II-VI semiconductors, such as the intense phonon-assisted edge-emission peaks in CdS; it also causes perturbations on the ground state energies of excitons and hydrogenically bound donor electrons, as well as frequency dependent changes in electron effective mass, all of which can become appreciable in the presence of externally applied magnetic and electric fields. All of these perturbations depend on the strength of the electron-phonon interaction which is determined by the energy band, lattice and dielectric parameters of a particular material. The electron-phonon interaction in polar semiconductors is essentially an induced-polarization phenomenon which is caused by the motion of an electron through the polarization field of the lattice ions. When a free conduction electron is set in motion, either thermally, or by externally applied electric and magnetic fields, there is an induced polarization field which couples to the lattice polarization field (phonon field). The induced polarization field (dipolar field) is equivalent to an electron-phonon scattering interaction and follows the electron as a polarization wave in its motion through the lattice. This polarization wave has the manifestations of mass and size and is thus a quasiparticle called the polaron; it also "dresses" the mass of the moving particle and, in effect, causes an increase in the electron effective masses in polar semiconductors.

The quantized Frohlich Hamiltonian, which describes the energy of a free electron moving in the periodic potential of a polar crystal lattice and coupled to the lattice through the induced polarization field (dipolar field), can be written as

$$H = \sum_{\underline{q}} \hbar\omega_{LO}(b^+_{\underline{q}} + b_{\underline{q}} + 1/2) + \frac{P^2}{2m^*} + \sum_{\underline{q}}(D_q b_q e^{i\underline{q}\cdot\underline{r}} + D^+_{\underline{q}} b^+_{\underline{q}} e^{-i\underline{q}\cdot\underline{r}}),$$

(44)

where, $D_{\underline{q}}$, the electron-phonon interaction coefficient, is given by

$$D_{\underline{q}} = -i \frac{\omega_{LO}}{q} \left(\frac{\hbar}{2m^*\omega LO}\right)^{1/4} \left(\frac{4\pi\alpha}{V}\right)^{1/2} \ldots$$

(45)

and α, the dimensionless Frohlich polaron coupling constant is defined by

$$\alpha = \frac{e^2}{} \left(\frac{1}{\varepsilon\infty} - \frac{1}{\varepsilon_s}\right) \frac{m^*}{2\omega_{LO}}^{1/2} \ldots$$

(46)

The other parameters, ω_{LO}, m^*, V, $\tilde{\varepsilon}\infty$ and ε_s are, respectively, the LO phonon frequency, the bare band electron effective mass, the crystal volume, and the high frequency and static dielectric constants. The first term of the Hamiltonian is the energy of the phonon field alone, the second is the kinetic energy of the electron and the third represents the quantized electron-phonon interaction, H_I, in terms of the electron position vector, $\underline{r}$, and the phonon wave vector, $\underline{q}$,

where,

b+$_{\underline{q}}$ and b$_{\underline{q}}$ are, respectively, phonon creation and annihilation operations which raise and lower the phonon quantum numbers by unity. b$_{\underline{q}}$ corresponds to the scattering of a free electron from a state of wave vector $\underline{K}$ to $\underline{K} + \underline{q}$, in which momentum is conserved by destroying a phonon of wave vector $\underline{q}$; conversely, b+$_{\underline{q}}$ corresponds to free electron scattering from $\underline{K}$ to $\underline{K} - \underline{q}$ with the creation of a phonon of wave vector $\underline{q}$.

As the above expressions indicate, the electron is coupled to the one-phonon states of the LO mode phonons of the lattice, and the strength of the electron-phonon interaction in a given material is determined by α, which can be calculated from the above formula. Bound electrons are also characterized by electron-phonon interaction in polar semi-conductors, and the interaction Hamiltonian, H_I, is of the same form as that given above. It is this interaction which gives rise to the phonon-assisted edge-emission lines in the II-VI compounds, as well as other very striking extrinsic phenomena, such as the localization of phonon states at impurity sites. We give below two examples which have been observed in the present work on CdS bound exciton photo-luminescence spectroscopy at cryogenic temperatures:

37

AFAL-TR-76-147

(1) The observation of phonon-assisted stokes and
antistokes transitions of a bound exciton complex
transition, in which the phonon-assisted transitions
were produced by the strong electron-phonon scattering
interaction in this material (~ 0.7) and by a non-
thermal distribution of LO phonons at low temperature.

(2) The observation of a hydrogenic bound-phonon quasi-
particle, in which the LO phonon states were localized
(bound) to the site of an acceptor impurity, to which
and exciton was also hydrogenically bound. This complex
was created by the strong electron-phonon interaction in
this material.

SECTION IV

MAGNETO - OPTICAL PROPERTIES

1. INTRODUCTION

Michael Faraday discovered the first magneto-optical effect in 1845. The effect which bears his name (Faraday rotation) was discovered when he observed that the plane of polarization of light transmitted through glass was rotated by an externally applied magnetic field whose direction was parallel to that of the light. Faraday's discovery rapidly spread to experiments in other materials, particularly gases, and lead up to the discovery of the Zeeman effect in gaseous atomic spectra in 1896. By the early years of the twentieth century, following the formulation of electro-magnetic theory by Maxwell and of dispersion theory by Lorentz, Drude, Voigt and others, the magneto-optical effect of dielectric media were remarkably well understood in terms of the classical dynamics of an electron in a magnetic field.

The first observations of resonant magneto-optical effects in semiconductors date back to the early 1950's, when microwave cyclotron resonance absorption of free electrons and holes was observed by Dresselhans, Kip and Kittel in Ge and Si. Cyclotron resonance soon proved to be a very powerful technique for probing the details of the energy band extrema in semiconductors, particularly in conjunction with the known quantum mechanical interpretations of the energy band structure, such as the effective mass approx-imation. In 1956, microwave cyclotron resonance was extended to the higher frequencies of the far infrared primarily resonance measurements and studies of the carrier effective masses and band structure in InSb. It was also in the mid-1950's that the first observations of the Zeeman effect in semiconductor impurities were observed, mainly from cyclotron resonance measurements.

Zeeman effects in the free excitons of the II-VI compounds (CdS and CdSe) were first observed by Thomas and Hopfield and by Wheeler and Dimmock, during the early 1960's, Thomas and Hopfield were also the first to observe the Zeeman effect in the bound exciton complexes of CdS (1961-62), and these observations were soon extended to several other II-VI compounds by Reynolds, Litton and Collins. In this section we will briefly review the magneto-optical properties of the II-VI compounds which have been measured from cyclotron resonance and bound exciton Zeeman spectroscopy.

2. EXPERIMENTAL FACILITIES

In addition to the spectroscopic and cryogenic equipment described in Section II-2, the magneto-optical facilities employed

in this work included a conventional, electromagnet capable of
producing steady magnetic fields up to 45KG. A modified version
of the high resolution grating spectrograph, whose limiting
spectral resolution was twice that of the one described in
Section III-2, was also employed in the magneto-optical facility.
The limiting resolution of this instrument was 0.04 cm^{-1}, the
magnetic field of this facility could also be extended to 110KH,
2.25" bore and a 1.25" diameter transverse optical access.
The magneto-optical facility was available to the task effort
and was employed mainly for magneto-optical spectroscopy in the
II-VI compounds. It was used in particular for photoluminescence,
absorption and reflection spectroscopy in high magnetic fields
and for the study of the Zeeman effect in free and bound excitons
and impurities. Also available to the effort was a magneto-
Raman spectroscopic facility. The apparatus assembled in this
facility comprised a high-resolution, double-pass Raman spec-
trometer, several high power pump lasers (visible and near I.R.),
photoelectronic detectors and signal processing electronics,
and the helium-cooled superconductive magnet solenoid. This
facility was employed in the measurement and study of spin-flip
Raman scattering in several of the II-VI compounds, discussed
in Section IV-4. Some of the far infrared cyclotron resonance
of the MIT National Magnet Laboratory. Spectral measurements were
performed at cryogenic temperatures in the MIT facilities, using
either a Fourier transform spectrometer, or a submillimeter laser
spectrometer. Both of these spectrometers were used in conjunction
with high-field Bitter magnet solenoids which produced steady
magnetic fields up to 200KG.

3. MAGNETO-OPTICAL SPECTROSCOPY

a. Zeeman Spectra of Intrinsic Excitons

We will now consider the case of an intrinsic exciton in
an externally applied magnetic field. The magneto-optical spectrum
of the exciton is very similar to that of the hydrogen atom.
Within the effective mass approximation of simple spherical energy
bands, the exciton Hamiltonian is equivalent to that of the hydrogen
atom. The Schrodinger equation of stationary excitons ($\underline{K}=0$)
in a static magnetic field, H. can be written as

$$\left[\frac{h}{2\mu} \nabla^2 + \frac{ieh(m_e^* - m_n^*)}{2c \, m_e^* \, m_n^*} \underline{H} \cdot \underline{r} \times \nabla + \frac{e^2}{8\mu c^2} (\underline{H} \times \underline{r})^2 - \frac{e^2}{\varepsilon_s \underline{r}} \right] \Psi \, exm \, (\underline{r})$$

$$= E\Psi exm \, (\underline{r}) \, . \, . \, . \quad (47)$$

where the wave functions, exm $(\underline{r})$, are highly restricted and refer only to the relative motion of the hole and electron. For the case of moving excitons ($\underline{K} \neq 0$), the wave functions) are complicated, due, in part, to the modification of the block functions by the magnetic field. This leads to complications in the solutions of the wave equation, and such excitons will not be considered here, since they are not characteristic of the II-VI compounds, when H is small, the field produces splittings and shifts of the exciton states similar to those of the atomic Zeeman effect. The second term of Equation (47) gives rise to a linear splitting in H for all states of non-zero angular momentum, and the third term a quadratic shift of all states, usually referred to as the dimagnetic shift.

For H=0, Equation (47) yields the hydrogenic solutions of the intrinsic exciton discussed in the previous section. The ground state wave function is 1s - like and can be written

$$\Psi_g (\underline{r}) = a_1^{3/2} \exp (\underline{r}/a_1) \dots \tag{48}$$

where

$$a_1 = \frac{\varepsilon_s \hbar^2}{e^2 \mu} = (m^*/\mu) \varepsilon_s \text{ ao} \qquad \dots \tag{49}$$

in which a_1 and a_o are the first Bohr radii of the exciton and the hydrogen atom, respectively. For small magnetic fields, the terms involving H can be treated as a perturbation. As noted above, the term linear in H has no effect on the ground state, while the H^2 term produces an energy shift in the ground state. This energy shift is given by

$$E(H)-E(o) = \frac{e^2 H^2}{8c^2 \mu} \left\langle r^2 \sin^2\theta \right\rangle = \frac{e^2 a^2}{4c^2 \mu} H^2 = \frac{e^2 a^2}{4c^2 \mu} \left(\frac{m^*}{\mu}\right)^3 \varepsilon_s^2 H^2 \dots \tag{50}$$

In solving Equation (47), it is convenient to consider a dimensionless magnetic field parameter, γ, which is the ratio of the magnetic energy of the exciton to its Coulomb binding energy. γ is given by

$$\gamma = \hbar\omega_c/2R_{ex}^* \qquad \dots \tag{51}$$

where R_{ex}^* is the exciton binding energy (effective Rydberg), and $\omega_c = eH/m^*c$ (the cyclotron frequency of the free electrons). The effective Rydberg is given by $R_{ex}^* = R(\mu/m^*)(1/\varepsilon^2 s)$, and the hydrogenic Rydberg, $R = 13.6$ eV. Making these substitutions, the energy shift of the ground state can be written in terms of

$$E(H) - E(0) = R(ao/e^2)\gamma^2 \qquad \cdots \quad (52)$$

Solutions of Equation (47) have been considered for three different ranges of γ: a low-field region, $\gamma \ll 1$; an intermediate region, $\gamma \sim 1$; and a high-field region, $\gamma \gg 1$. Approximate solutions which are in reasonably good agreement with experiment have been obtained for both the high and low-field regions. For example, Elliot and London have obtained numerical solutions for $\gamma \gg 1$, in reasonably good agreement with experiment. The intermediate region $\gamma \sim 1$, is difficult to treat theoretically, and exact solutions have not been achieved. For example, perturbation theory becomes invalid for $\gamma \sim 1$. One of the difficulties in treating both the low- and intermediate-field regions is to properly account for the continuum states in the presence of the Coulomb interactions of the exciton; another is the appearance of quantum mechanically forbidden level-crossings which occur in the hydrogenic model at low magnetic fields. Hopfield has, however, achieved a satisfactory theoretical treatment of the low-field region for the anisotropic exciton structure of CdS· the results of his variational calculation are summarized in the review of Refs. 9 and 10 cited in the Appendix of this report.

The solutions of Equation (47) yield the magnetic energy levels of the intrinsic exciton which are characterized by three quantum numbers, n, i, m. For a given n and i, m=0 corresponds to the lowest energy state (in the absence of spin) and is given by

$$E^{n,i} = (2n + 1) R^*_{ex}\gamma + E_z^{n,i} \quad \cdots \qquad (53)$$

The quantum number n is associated with the electron Landau levels, while the quantum number i is associated with exciton orbital motion parallel to H. For example, n=i=0 corresponds to the ground state. The term E_z is the energy separation between the exciton level and the associated Landau level.

We have not included spin terms (electron or hole) in the exciton Hamiltonian of Equation (47). When spin is included it produces a spin-degeneracy in the exciton states which is lifted by the applied magnetic field. In sufficiently high magnetic fields, spin-splittings are observed in typical intrinsic exciton spectra. They are in, general, defined by $\Delta E_{e,h} = g^*_{e,n} \beta H$, where $g^*_{e,n}$ is the effective g-factor of the electron or hole and β is the Bohr magneton ($\beta = eh/2m_o c$).

The excitonic Zeeman states which we have considered above are those of simple isotropic excitons which derive from simple isotropic energy bands. In the case of the wurtzite structured II-VI compounds, we must consider the Hamiltonian which describes the anisotropic exciton parameters of these materials in a magnetic field. We must then solve the wave equation for this Hamiltonian which does not have closed-form solutions. From approximate solutions to the wave equation, Thomas and Hopfield and Wheeler

and Dimmock have obtained calculated values of the magnetic states as a function of magnetic field for the anisotropic excitons of Cd5 and CdSe. Their calculated values are in very good agreement with those deduced from the experimental spectra of these materials. We have used their theoretical results in our magneto-optical studies of the intrinsic exciton structure in the wurtzite II-VI compounds.

b. Zeeman Spectra of Bound Excitons

As we showed in Section III-6, semiconductor defects and impurities, such as neutral donors or acceptors or ionized donors or acceptors, can capture free excitons to form molecular-like complexes at low temperatures. Bound exciton complexes are observed in photoluminescence spectra predominantly, but also appear weakly in absorption. In the presence of a magnetic field, these bound exciton complexes give rise to unique Zeeman spectral patterns which are characteristic of the particular type of semi-conductor defect to which the free exciton is bound. In case of the wurtzite structured II-VI compounds, these bound excitons are highly anisotropic and the splittings of their magnetic states depend strongly on the angular orientation of the crystalline c-axis with respect to the direction of the magnetic field. Several examples are illustrated below, in which the host crystal is in a static magnetic field of strength H, oriented such that $E \perp C$:

| Exciton Bound to Neutral Donor (a) | Exciton Bound to Neutral Acceptor (b) | Exciton Bound to Ionized Donor (c) |
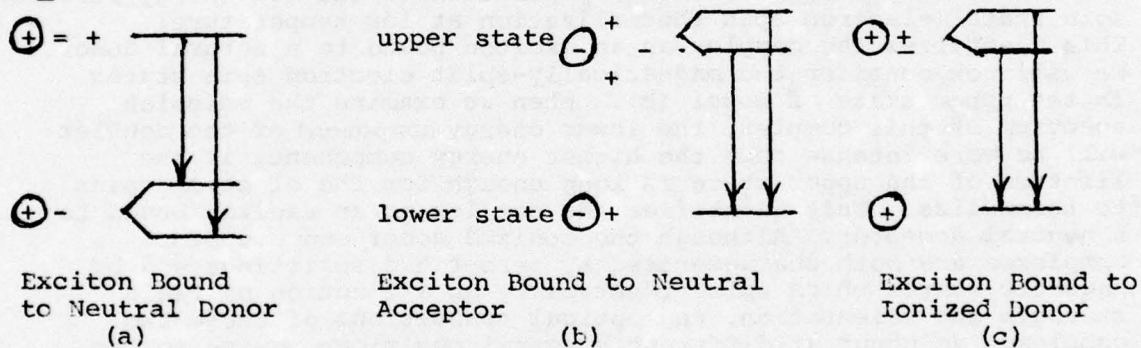
In examples (a) and (b), neutral donor and neutral acceptor, the unpaired electron spin splitting is isotropic, while the unpaired hole spin splitting is anisotropic, so that we may write for the g-factor of these states

$$g = g_e \text{ (isotropic)}$$

$$g = g_{h11} \cos \theta$$

where θ is the angle between the crystal c-axis and the direction of the magnetic field and g_{h11} is the hole g-factor when H11C. For any arbitrary orientation of the magnetic field with respect to the c-axis, the upper state of the neutral donor complex (a) will split into two states so that four transitions are observed; under the same conditions, the lower state of the neutral acceptor complex will split into two states so that four transitions are also observed in this case. However, in the H$\perp$C orientation shown above, the hole spin splitting is quenched, since cos θ = 0 at H$\perp$C. Thus, only two transitions are observed for the neutral donor complex at H$\perp$C, and similarly for the neutral acceptor complex. The magnetic states and the spin splitting of the ionized donor complex (c) and the ionized acceptor complex are identical. At C$\perp$H, both the ionized donor and the ionized acceptor complexes are zero-field split by a spin-spin exchange interaction, giving rise to two transitions at both H=0 and at finite values of the magnetic field strength. But at any arbitrary orientation of H with respect to C ($0<\theta<90^\circ$), the upper states of the ionized complexes split into four states and four transitions are predicted.

We return now to the donor and acceptor complex models illustrated in (a), (b), (c) above for H$\perp$C. When we examine the absorption spectrum for the model (a), we observe that the higher energy transition is more intense than the lower energy transition, which is due to the preferential population of the low-energy electron spin state (electron spin thermalization at low temperature). This identifies the complex as an exciton bound to a netural donor. We will now consider the magnetically-split electron spin states in the upper state of model (b). When we examine the emission spectrum of this complex, the lower energy component of the doublet will be more intense then the higher energy component, if the lifetime of the upper state is long enough for the electron spins to thermalize. This identifies the complex as an exciton bound to a neutral acceptor. Although the ionized donor and acceptor complexes are both characterized by zero-field splittings and by magnetic states which split identically as a function of field strength and orientation, the optical transitions of these two complexes do occur at different spectral positions, owing to the differences in their binding energies. Thus, from determinations of spectral position and intensity at known crystal orientations in a magnetic field, it is possible to differentiate between neutral donor and neutral acceptor complexes, between ionized donor and ionized acceptor complexes and between neutral and ionized complexes. It is not possible, of course, to identify the chemical origin of the donor from such Zeeman spectra, but this can often be done through selective impurity doping in conjunction with bound exciton spectroscopy. Bound exciton spectroscopy has been a very powerful analytical tool in the present work on impurity and defect characterization in the II-VI compounds, not only in the wurtzite

structures described above, but also in several of the Zincblende crystals. Some of the characteristic bound exciton photolumines- cence lines observed in CdS and CdSe are listed in Tables VI and VII. The I_1 (neutral acceptor) and I_2 (neutral donor) lines are now believed to be due to native defects, i.e., stoichiometric defects in the CdS crystal lattice.

c. Infrared Cyclotron Resonance

Far infrared cyclotron resonance absorption studies have been performed in a number of narrow and wide bandgap semicon- ductor materials, such as InSb and InAs and CdTe and GaAs, during the course of this work. These studies have been confined to intra-conduction-band cyclotron resonance spectral measurements of free electrons, and have also included far infrared magneto- spectroscopic studies of shallow donor impurities in these materials.

Cyclotron resonance spectroscopy is a very powerful exper- imental technique for probing the details of the electronic band structure in semiconductors, and also provides more precise and reproducible values of the charge-carrier effective masses (hole and electron) than can be obtained by any other experimental method, including electrical transport measurements. The allowed infrared cyclotron resonance transitions between conduction band Landan levels, determined by the cyclotron resonance frequency,

$$\omega_c = eH/m^*c$$

and the magneto-optical selection rules, have been measured over a wide range of fields, frequencies and temperatures in high mobility InAs and CdTe single crystals. The cyclotron resonance measurements have provided accurate values of the electron effec- tive mass and its dependence on magnetic field and temperature in these two materials. In InAs, for example, low-field, low- temperature electron effective masses as low as $m^*/mo = 0.0223 \pm 0.0002$ have been measured from cyclotron resonance absorption in high-mobility ($\sim100,000$ cm^2/v-sec at 77°K) n-type epi-taxial layers. Moreover, the rise in electron mass (polaron mass), due to electron-phonon interaction and conduction band non- parabolicity, has been measured from microwave frequencies ($\lambda = 1mm$) up to the LO phonon frequency ($\lambda - 41$ μm) in the InAs epi-layers. Accurate values of the electron g-factor and its magnetic field dependence have also been determined for this material. Similar effective mass measurements have also been performed on n-CdTe specimens of high mobility ($\mu = 100,000$ cm^2/v-sec at + 40°K). Electron effective mass changes due to polaron effects have been measured to a very high precision for the first time in CdTe and this will be discussed in Section IV-5.

The far infrared cyclotron resonances transitions of the shallow donor impurity in InAs were observed for the first time in the present work. Several of the allowed hydrogenic donor transitions, such as the 1s→2p, 1s→3p and 1s→4p (m=±1, 0), were observed in absorption resonance spectra and have been studied as a function of magnetic field and temperature. Several of the excited state transitions were also observed and a chemical shift was observed in the 1s-2p, m=1 transition, indicating the presence of at least two shallow hydrogenic donors of nearly the same binding energy. The optical absorption spectrum of the shallow donor is hydrogen-like in most of the II-VI and III-V compounds. Moreover, the magneto-optical absorption spectrum of the shallow donor is very similar to that of the intrinsic exciton in a magnetic field, discussed in Section IV-3b. The zero-field binding energy of the shallow donor in the InAs can be calculated from the hydrogenic Rydberg formula, from which we obtain

$$R^* = R(m^*/m_0)(1/\varepsilon_s^2) = 11.5 \text{ cm}^{-1}$$

From this value of the binding energy, we calculate 8.6 cm^{-1} for the 1s→2p transition energy. This is in reasonably good agreement with the value, 9.5 cm^{-1}, obtained by extrapolating the experimentally measured transition energies between the magnetic states back to zero magnetic field. Similar magneto-spectroscopic measurements of the shallow donor impurity transitions have also been made in CdTe over a wide range of frequencies.

4. Spin-Flip Raman Scattering

Ever since the spin-flip Raman laser was first demonstrated by C.K.N. Patel at Bell Telephone Labs, there has been a rapidly growing interest in this magneto-optical phenomenon in semiconductors. The success of the InSb SFR laser, as a source of magnetically-tunable, coherent radiation over the 5 to 15 μm spectral region (pumped with CO_2 and CO gas lasers), has led naturally to a search for other semiconducting materials which could be pumped to stimulation with existing lasers. Unlike InSb, whose $g_e^* \sim -50$, the wide bandgap II-VI semiconductors (visible to near I.R.) have rather small Landau level spin-splittings ($g_e < 2$), owing to the fact that their conduction and valence band spin-orbit interactions are not large compared to their bandgaps. Spin-flip scattering is still possible to these materials; we require only that the spin-orbit coupling be finite, plus an external field to split the spin states by

$$\hbar\omega = g\beta H$$

where β is the Bohr magneton. In practice, however, high resolution spectroscopy is required to analyze the SF scattering.

The research in this task on spin-flip Raman scattering was confined primarily to the II-VI compounds, such as CdS, CdSe, CdTe and ZnSe, and was directed primarily toward characterizing the spin-flip scattering process in these materials, as well as investigating the possibilities of magnetically tunable laser sources in the visible and very near infrared.

Spontaneous spin-flip Raman scattering has been observed in CdS, CdTe, CdSe and GaAs. Both stokes

$$\omega_S = \omega_L - g\beta H,$$

and antistokes,

$$\omega_A = \omega_L + g\beta H,$$

peaks were observed in these materials, separated from the laser pump frequency, ω_L, by $g\beta H$, the Landau level spin splitting. The spontaneous scattering in CdS is from both free and bound electrons, the latter process giving rise to intense and extremely narrow spontaneous line widths, ~ 0.001 cm^{-1} or less. When pumped with the 4880 Å or the 5145 Å lines from an argon ion laser, the CdS stokes scattering peak can be tuned over a range of some 5 Å in wavelength, about the laser center frequency. Stimulated scattering has also been observed in CdS by Scott. The observed spontaneous scattering in CdTe, CdSe and GaAs was from free electrons, and all measurements were performed at low temperatures.

Electron g-factors for CdS, CdTe and CdSe have been calculated from the measured spectral positions of the stokes and antistokes spin-flip peaks, over a range of magnetic fields between 30 and 100 KH. The g-factors were calculated from the relations,

$$g = (\omega_L - \omega_S)/ H\beta, \quad \text{or} \quad g = (\omega_A - \omega_S)/2\beta H,$$

and were nearly constant with magnetic field. The present spin-flip Raman scattering g-factor measurements are summarized in Table VIII, together with those determined by other methods, such as exciton magneto-optics, EPR and NMR. The present work has yielded the first direct measurement of the electron g-factor in CdTe, as well as an experimentally measured g-factor for GaAs which is in excellent agreement with the value determined from EPR. The spin-flip scattering in CdTe, CdSe and GaAs was pumped with a Nd:YAG laser at 1.06 µm.

5. Polaron Cyclotron Resonance

Over the past several years, infrared cyclotron resonance has been employed to prove the electron-phonon interaction in

47

polar semiconductors, such as the III-V and II-VI compounds. These studies have concentrated on the intraband cyclotron resonance transitions between n=0→n=1 and n-1→n-2 Landau levels. Cyclotron resonance in polar semiconductors is called polaron cyclotron resonance because it is the "dressed" polaron mass, rather than the free electron mass, which is observed in cyclotron resonance transitions in these materials. The fact that the electron-phonon interaction perturbs the free electron Landau levels in a theoretically predictable way has made it possible to quantitatively determine the effects of polaron formation in a number of polar semiconductors.

The Fröhlich electron-phonon interaction Hamiltonian was discussed in Section III-7. Wave mechanical solutions of this Hamiltonian, using perturbation theory, yield the polaron-induced changes in electron energy levels and effective mass, which are due to the electron's motion through the polar lattice and which have been observed experimentally. For example, the Fröhlich electron-phonon interaction theory predicts that the free polaron mass, m**, is related to the free electron effective ma-s, m*, by

$$m^{**} = m^{*}(1 + \alpha/6),$$

where α is the dimensionless Fröhlich polaron coupling constant, defined in Section III-7. If the free electron effective mass and the coupling constant are known, then the free polaron mass can be calculated. Unfortunately, the truly free electron mass is not known, since it can not be measured directly from experiments in polar crystals, i.e., it is always dressed by polaron coupling even at very low energies. To a very good approximation, however, we can assume that the low-temperature effective mass measured at millimeter microwave cyclotron resonance frequencies is the same as the free electron effective mass, since polaron coupling is negligible at these low frequencies. There are also difficulties in calculating accurate values of the polaron coupling constant, α, from the formula given in Section III-7 and the known values of the dielectric and optical constants of the material. It is actually much better (and more precise) to determine the polaron-induced changes in effective mass from cyclotron resonance spectra in conjunction with polaron cyclotron resonance theory, as has been done in the present work on CdTe. A precise value of the coupling constant, α, can then be obtained by fitting the theoretically calculated polaron effective masses to those measured from cyclotron resonance spectra, since the theoretical values are calculated as a function of magnetic field and coupling constant.

In the case of cyclotron resonance, the motion of the electron through the polarization field (phonon field) of the lattice is

provided by the orbital motion of the cyclotron electron whose orbital frequency is precisely controlled by the applied magnetic field strength. In order to account for the cyclotron motion in the Frohlich Hamiltonian, we must replace the electron kinetic term, $p^2/2m$, by a kinetic energy term which expresses the electron momentum in terms of the vector potential of the radiation and the applied magnetic field. It is this Hamiltonian which precisely predicts the polaron-induced shifts in cyclotron frequency and effective mass which have been observed experimentally.

Several very striking manifestations of electron-phonon interaction are observed in the cyclotron resonance spectra of polar semiconductors. When the cyclotron frequency, ω_c, approaches the LO phonon frequency, ω_{LO}, the electron-phonon interaction becomes very strong and resonant polaron effects are observed. For $\omega_c = \omega_{LO}$, there are pronounced shifts in the cyclotron frequency and the effective mass. When ω_c passes through $\omega_{LO}(\omega_c > \omega_{LO})$, there is a very striking increase in the linewidths of the cyclotron resonance absorption peaks. These effects have been observed in the present magneto-optical studies of InAs and InSb. At fields and frequencies below ω_{LO}, it is possible to make quantitative measurements of the magnitude of the electron-phonon interaction. For example, the electron-phonon interaction causes a rise in the free electron mass as the frequency (ω_c) and field rise from zero toward the phonon frequency (ω_{LO}). This increase in mass (polaron mass) causes a deviation of the cyclotron frequency from the usual linear relation between the resonant field and frequency, determined by the cyclotron resonance equation

$$\omega_c = eH/m^*c$$

The resonant absorption frequency and field can be measured directly and the increase in mass can be calculated from the cyclotron resonance equation. Masses determined in this way are polaron masses. In CdTe, for example, millimeter microwave CR measurements yield a free electron effective mass of $m^*/mo - 0.0963 \pm 0.0008$ (at $4°K$). At submillimeter laser frequencies (for infrared), the effective mass (polaron mass) rises to $m^*/mo = 0.1124 \pm 0.0005$ at a frequency $\omega_c = 128$ cm^{-1} ($\lambda = 78$ μm, $H = 155$ KG), which is within 25% of the LO phonon frequency at $\omega_{LO} = 170$ cm^{-1}. This represents a 15% increase in effective mass, of which 2% is due to the effect of conduction band nonparabolicity in this material. Thus we find that the electron-phonon interaction in CdTe produces a 14% increase in the free electron effective mass, when the electron is moving through the lattice at an orbital frequency corresponding to about 75% of the LO phonon frequency. Clearly, this is an appreciable change in the electron effective mass, and since it arises from an intrinsic property of the crystal, it can not be ignored. From these data we have also put the experimental value of the electron-phonon coupling constant in CdTe at $\alpha = 0.40 \pm 0.03$.

Section V

DEVICE ORIENTED RESEARCH

For a number of years, it has been the operating philosophy of the Solid State Physics Research Laboratory to pursue a strong in-house program of basic research in selected areas of semi-conductor physics, primarily in the II-VI compounds, and, at the same time, to support and pursue research aimed at device development in a few promising areas of interest to the Air Force. Device oriented research efforts have been generated either from ideas which grew out of the in-house research program, or from known research needs within the Air Force R&D Program. Several examples of device oriented research which have been pursued and/or supported under this task effort are presented below. One of these, CdS Solar Cell research and development, is a direct out-growth of the in-house research program; another is in direct response to a high-priority Air Force need in the area of high-power infrared laser window materials required for weapons technology.

1. $CdS:Cu_2S$ SOLAR CELLS

The photovoltaic effect was first observed in silicon in 1953 by workers at the Bell Telephone Laboratories. This discovery later led to the rapid development of the silicon solar battery, particularly as the auxiliary electrical power sources for space satellites. In the following year, 1954, Reynolds was the first to observe the photovoltaic effect in $CdS:Cu_2S$ hetero-junctions; this was followed in the same year, by his invention and demonstration of a working model of the single-crystal CdS solar battery. These early discoveries have led to a steadily increasing interest in this type of solar energy converter, not only for space applications, but also for terrestrial applications. For several reasons, however, the silicon solar cell largely overshadowed the CdS cell for more than two decades, primarily because its conversion efficiency has been approximately twice that of the CdS cell and because of its extensive development for space applications. An additional factor which favored the development of the silicon cell was the fact that much of the semiconductor technology required for its development was already on hand at the time of its invention, or soon became available from the enormous R&D effort on silicon transistor technology which was being developed in the late 1950's and early 1960's. Fortunately, however, during the time period 1955-1956, the first successful polycrystalline CdS film cell was achieved by the Clevevite Co., under contract supported by ARL. This

represented an important technological breakthrough, since it demonstrated for the first time that it would be possible to ultimately produce cheap, light-weight, large-area solar cells for both space and terrestrial applicatons. It was also clear that such solar cells could make possible the large area arrays required for practical electrical power generating stations. The early CdS film cells were vacuum evaporated on various types of electrode materials and supporting substrates, with chemically deposited CuS barrier layers and various collector grid materials. Typically, they had an active area of approximately 9 in^2 (3" x 3"). In addition to its light-weight, the CdS film cell was also flexible which made it attractive for the power generating arrays required for space vehicle applications. Silicon, on the other hand, has always been a single crystal solar cell and single panels of large power arrays comprise literally hundreds of single crystal cells, which make such arrays not only heavy, but also very expensive to produce. NASA actually supported a very modest program of research and testing of CdS film cells (for possible space applications) during the mid- to late-1960's but, in spite of this fact, the CdS film cell never became a serious competitor to silicon for this purpose. In a program organized and sponsered by ARL, during the mid- to late-1960's, several CdS film cells were life-tested in the vehicles: OV113 and OV117. The data from these experiments showed that the performance of the CdS cells was only slightly degraded after more than 18 months of operation and that their performance degradation was less than that of silicon cells under identical conditions.

This task effort has supported several years of continuing research on the improvement of conversion efficiency and performance of the CdS:Cu$_2$S film cell, mostly performed under contract with the Clevite Corp. and later with the Gould Corp. Over the years, the output efficiencies and performance of the CdS cell have steadily improved. For example, short circuit current and open circuit voltage maxima have risen steadily to values as high as 800 - 900 mA and 500 mV, respectively, in 3" x 3" cells; conversion efficiences of 5 to 6% are routinely achieved and occasionally cells of 7 to 8% efficiency are produced. Many other problems concerned with cell stability, reliability and failure have been systematically solved through painstaking research and engineering efforts. Much effort has also been given to purification and removal of defects in the materials from which the cell is fabricated, in particular the n-type CdS layer and the extremely thin p-type Cu$_2$S layer from which the barrier layer (heterjunction) is formed. A great deal of effort has been focused on achieving a better understanding

of the barrier layer itself, particularly the charge-carrier transport mechanisms and the presence of surface states at the junction. It has been shown recently by the Phillips Laboratory group that the relatively low efficiency in the early film cells can be traced to a deviation in stoichiometry in the Cu_2S layer. There is evidence that precisely stoichiometric Cu_2S layers lead to cell conversion efficiencies exceeding 10%. The CdS solar energy converter is an excellent example of how basic research and a better understanding of materials, particularly in the II - VI compounds, have led to the development and production of an extremely useful device. And much of this better understanding of materials, which has made the CdS cell possible, has come from the basic research efforts of ARL, over the past decade and more.

Interest in the CdS film cell has dramatically increased during the past two years, primarily because it now appears that the CdS film cell will be the more economical alternative, amongst several possible materials (including silicon), for terrestrial applications, particularly for the production of electrical power in solar houses and for the large solar cell areas required for commercial electrical power generating stations. Work on the further development of the CdS film cell for large scale electrical power generation and for solar houses is now underway in several institutions, including the University of Delaware (Institute for Energy Conversion), Brown University, Westinghouse Research Labs, Baldwin Research Labs, Solar Energy Systems (a division of Shell Oil Co.) and several others. In light of the national energy crisis, it seems to us that the CdS solar cell is an idea whose time has come, some 20 years after its invention! It also seems to us that the funds and resources expended on the research and development of this solar cell will ultimately serve a very important national purpose, and the Air Force will undoubtedly reap considerable benefits as well.

2. HIGH POWER INFRARED LASER WINDOWS

Since early 1971, approximately 30% of the task effort has been devoted to a high-priority program on research and development of High Power Infrared Laser Window Materials, with particular emphasis on window materials for the high power CO_2 laser which radiates at 10.6μm wavelength. This rather extensive program is continuing under the joint sponsorship of the AF Weapons Laboratory (Kirtland) and the AF Materials Laboratory (WPAFB), and has included the participation of ARL and AFCRL, several Army

and Navy research labs, and a number of university and industrial laboratories. The primary contribution of this task effort has been that of crystal growth, laser window sample preparation and spectroscopic analysis of window samples.

When the high power CO_2 laser window program began, several groups of insulator and semiconductor materials, such as the alkali halides, the II - VI compounds and the III - V compounds, were thought to be potential window materials. At that time, very little was known about the transmission of intense infrared radiation through the alkali halide materials, which had long been used for low-power, near-infrared transmission optics, and even less was known about the high power density transmission capabilities of the II - VI compounds in the near infrared spectral region. In spite of this fact, ARL scientists were among the first to suggest that CdTe, CdSe and ZnSe crystals ought to be promising candidates for the CO_2 laser window application and agreed to test this speculation by establishing a program for the growth of large, high-purity samples and to provide these samples to the AFML laser window testing program. Initially, large single crystal ingots of CdTe and CdSe were grown. From these ingots, window specimens up to two inches in diameter and 0.5 inches thick were cut and polished. Many of these window specimens were subjected to high power density tests in the beam of a c.w. CO_2 laser. Most of the CdTe and CdSe specimens were capable of transmitting power densities in the range of 2 to 3 kilowatts/cm and showed only a slight rise in temperature after several minutes in the beam. Only the poorest of these specimens sustained surface burn damage, due to beam absorption, and this could usually be traced to the presence of mechanical imperfections, such as grain boundaries and hidden cracks within the specimen. As the program progressed, even higher-quality, high-resistivity CdTe and CdSe window specimens were produced and many of these had measured absorption coefficients as low as $0.0009 cm^{-1}$ for CdTe and $0.0006 cm^{-1}$ for CdSe. Unfortunately, the mechanical strength of CdTe and CdSe single crystal window specimens was not very high, and this was particularly true of the CdSe specimens which were cut such that their crystalline c-axes were perpendicular to the specimen faces in order to preclude beam refraction effects due to birefringence. Eventually, the CdTe and CdSe window effort was abandoned, largely because of the relatively poor mechanical properties of the materials. At this point in the program, the Raytheon Co., one of the contractor-participants in the program, succeeded in growing large polycrystalline ZnSe window specimens of relatively low absorption coefficient by the chemical vapor deposition technique. Although the polycrystalline ZnSe window specimens did not have absorption coefficients as low as those

of single crystals, their mechanical strength was appreciably higher than that of single crystals, and it was reasoned that the advantage of higher strength would more than off-set the disadvantage of the lower absorption coefficient. As a result of this achievement, the techniques required for the vapor phase sublimation growth of polycrystalline ZnSe were developed and a rather extensive in-house program on the growth of polycrystalline ZnSe laser window specimens was begun. One of the objectives of this effort was to compare the relative merits of window specimens grown by the two techniques (CVD and vapor phase sublimation), particularly with respect to absorption coefficient, mechanical strength and the presence of foreign impurities and defects in the samples. Eventually, polycrystalline ZnSe window specimens were grown by the vapor phase sublimation technique with absorption coefficients in the range of 0.001 to 0.005cm^{-1}, comparable to those produced by the CVD technique. As part of this effort, single crystal ZnSe window specimens were also grown and tested, primarily for the purpose of making comparisons between the single and polycrystalline window specimens. Small, single crystal ZnSe window specimens were eventually produced with absorption coefficients as low as 0.0005cm^{-1}. Many of the CdTe and CdSe laser window specimens, as well as the single and polycrystalline ZnSe specimens, were supplied to AFML for their laser window characterization program, particularly for the determination of absorption coefficients, surface and bulk scattering losses, thermal conductivity and thermal loading characteristics, as well as mechanical strength and hardness tests.

The photoluminescence spectra of both the single and poly-crystalline ZnSe window specimens were also studied in consider-able detail at low temperature (1 to 4 degrees K). From the outse it was expected that only broad-band, phonon-assisted photo-luminescence peaks (due to recombination radiation of impurities and defects) would be observed, since past experience with the other II – VI compounds had shown that one could not, in general, expect to observe sharp bound exciton line omission in the photoluminescence spectra of single crystals which crystallized in the zincblende structure. Moreover, it was also not expected that sharp line emission would be observed in the imperfect lattices of the polycrystalline window specimens. Quite surprisingly, however, sharp line emission due to bound exciton and free exciton transitions were observed in the single crystal ZnSe specimens, and sharp line emission due to bound exciton complex transitions was also observed in the polycrystalline ZnSe specimens. This was the first time that such observations

had been made and the importance of it was recognized immediately. It meant that the bound exciton photoluminescence technique could be employed to analyze the residual impurities and defects in the ZnSe polycrystalline window specimens in great detail. It also meant that the impurity and defect concentrations could be examined over many small areas of a large window specimen, since the method is a non-destructive analytical technique. During the course of the photoluminescence measurements, bound exciton transitions were observed which were thought to arise from stoichiometric defects (presence of excess Zn and Se) in the ZnSe specimens. This was later confirmed through spectral measurements in conjunction with baking experiments, i.e., specimens baked in Zn and Se atmospheres. Other bound exciton transitions were also observed and identified tentatively with specific foreign impurities.

Although the alkali halide window, KCI, was employed in some of the early, low-power, CO_2 laser systems, polycrystalline ZnSe windows have now been selected for the final high-power CO_2 laser systems. And large multi-paned ZnSe windows have been recently fabricated for this purpose. It would also appear that polycrystalline ZnTe, and perhaps ZnSe:Te, could be developed for this purpose eventually. The results of the inhouse research on II - VI compound laser windows are summarized in several papers published in the Proceedings of the Air Force High Power Laser Window Materials Conferences, cited in the Appendix of this report.

3. NON-LINEAR OPTICS: GROWTH AND STUDY OF HgS CINNABAR

Red mercury sulfide (more popularly known as cinnabar or λ- HgS) is a wide bandgap semiconductor which is of considerable interest because its unique properties offer excellent potential for non-linear optical devices, particularly laser technology devices. It is the most optically active of all known mineral compounds, possessing the greatest birefrigence, a remarkable optical rotary power and strong piezoelectric properties.

It is also known that α- HgS has the highest acousto-optical figures of merit of any known crystalline material, making it an efficient material for acoustooptical applications, such as transducers, laser light modulators, deflectors, delay lines, etc. Since the electromechanical coupling coefficients of cinnabar are approximately twice those of quartz, piezoelectric α- HgS transducers bonded to a parallelepiped cinnabar crystal

would realize perfect acoustical matching and therefore yield
wide bands for acousto-optical deflection. Thus α - Hgs
should be a good deflector of laser light. For example, if
one assumes a frequency bandwidth of 250MHz for a cinnabar
transducer and an acoustic beam 0.5 mm square, it can be shown
that only 210 mW of acoustic power are necessary to deflect
all of the incident light of a 6328A He-Ne laser beam into
some 62500 different positions with an access time of 1 μs.

Of perhaps even greater importance are the strong non-
linear optical properties of cinnabar. Its measured d_{11} non-
linear coefficient is amongst the highest known for any of the
non-linear optical materials; in fact, its d_{11} coefficient is
exceeded only by those of crystalline Se and Te, which have
the highest coefficients of any known materials. Unfortunately,
Se and Te have rather small bandgaps and their transmission
is limited to the near infrared spectral region; cinnabar,
on the other hand, is transparent from the visible red (about
6000A) out to a wavelength of some 14 μm, which makes it a
more versatile non-linear optical medium for many applications.
Because of these properties, α - HgS has a great deal of po-
tential for non-linear optical device applications, such as
integrated optical circuits, parametric oscillator frequency
upconversion, difference frequency generation and tunable
lasers (angle tuning), to name but a few.

To date most of the fundamental optical and electrical
properties of α - HgS have been measured from natural crystals
which are not only small, but also exceedingly rare. The
natural crystals also contain large concentrations of foreign
impurities which make them undesirable for many laser appli-
cations, owing to their high extrinsic absorption of light.
In spite of their higher purity, it is, unfortunately, very
difficult to grow synthetic cinnabar crystals of usable size
in the laboratory. Over a period of many years, a number of
different investigations have tried unsuccessfully to grow
large synthetic cinnabar crystals by several different methods.
In most of these attempts, submillimeter-size crystals were
produced. Another difficulty encountered in the growth of
synthetic cinnabar is the fact that HgS undergoes a phase
transition at approximately 330 degrees C: above this tem-
perature cinnabar transforms to the black cubic structure
(α - HgS) which has a small bandgap and is of no interest for
non-linear optical applications. This requires that the red
form (cinnabar) be grown at temperatures below 330 degrees C,
a condition which severely limits the growth rate.

About three years ago (1971), several French investigators
succeeded in growing large synthetic crystals of α - HgS.
These crystals had volumes in excess of 1 cm (about 20 gms)
and were grown by the hydrothermal technique. The French success

has sparked a renewed interest in synthetic cinnabar crystals, primarily because of their great potential for application in laser optics technology. It was, in fact, responsible, for the present task effort on the study and growth of synthetic cinnabar crystals, which began about three years ago, and which has continued, in part, under Laboratory Director Funding for the past two years.

In the present effort, cinnabar crystals have been grown by a novel variation of the iodine transport technique. Typically, a 12'' long, 1.5" diameter quartz tube served as the source and growth chambers. The source material comprised some 50 - 150 gms of technical grade HgS mixed with about 5 mg/cc of I_2. The source material was then placed into the closed end of the tube. Following evacuation of the air from the tube, its open end was sealed off. This tube was then placed in a furnace such that a temperature gradient was maintained across its length, typically between 100 and 140 degrees C. The source material was maintained at temperatures between 400 and 440 degrees C and the colder end of the tube (growth region) was maintained at approximately 300 degrees C. The source material decomposed and reacted to form vaporous compounds which transported to the colder end of the tube (growth and reaction zones). The transport species, HgI_2 and S_8, reacted to form HgS, several weeks after a few grams of the compound Hg S I were deposited across the colder end of the tube. Both α - HgS and black (cubic) HgS crystals grew in separate regions of the colder end of the tube. Cinnabar crystals in thick platelet form as large as 5 x 4 x 1 mm and 7 x 2 x 1.5 mm were grown over periods of 50 to 60 days.

Bandgap energies of these synthetic cinnabar crystals, obtained from optical absorption measurements at temperatures between 300 to 4.2 degrees K, were in excellent agreement with those published in the literature, confirming the yield of good cinnabar crystals from the iodine transport technique. At room temperature, the bandgap of α - HgS falls at 2.10 eV; the temperature coefficient of its absorption edge is rather large, $\sim 9 \times 10^{-4}$ eV/degrees K, over the range 300 to about 20 degrees K. In the EllC mode of polarization, the bandgap falls at a wavelength of 6115A at room temperature. X-ray diffraction measurements of the lattice constants were also in excellent agreement with the published literature values, again confirming a yield of good quality cinnabar crystals by this growth technique. Far infrared transmission spectral measurements were also made in the neighborhood of the reststrahlen absorption band and several of the characteristic optical mode absorption frequencies (phonon frequencies) were observed, in very good agreement with published values.

SECTION VI

SIGNIFICANT ACHIEVEMENTS

During the course of this task effort a number of "firsts" in semiconductor physics were achieved. Several of these achievements are listed below without further comment except to say that they represent the original ideas and productive efforts of a number of scientists and technicians who worked, at one time or another, as part of the group effort. In most cases, these achievements have contributed either directly or indirectly to a better understanding of the fundamental and defect properties of a number of important semiconductor materials.

1. First observation of negative resistance characteristics and double-carrier-injection in Li- and Na-doped CdS single crystals.

2. First observation of spatial dispersion effects in the intrinsic exciton edge emission spectrum of CdS arising from polaritons; identification of spatial resonance dispersion effects in the intrinsic exciton reflection spectrum of wurtzite CdSe single crystals.

3. First observation of the vibrational spectrum of a bound exciton complex (observed in the emission spectrum of CdS, analogous to the classical vibrational spectrum of molecular hydrogen).

4. First characterization of the bound exciton spectral transitions of CdSe and ZnO single crystals: magneto-optical studies.

5. Identification of free excitons bound to preferentially paired donor and acceptor impurities in Li-doped ZnO emission spectra.

6. Magneto-optical identification of the bound exciton transitions which characterize the radiation spectra of CdS and CdSe Electron-Beam-Pumped Lasers (Provided the platelet single crystals required for the first observation of electron-beam-pumped laser action in CdS, CdSe and CdS:Se-observed at MIT Lincoln Lab).

7. First observation of excited terminal states of bound exciton donor complexes in CdS, CdSe and ZnO.

8. One of the first observations of donor-acceptor pair recombination spectra in CdS, including magneto-optical characterization of the states of such impurity complexes.

9. First growth of low-absorption-coefficient CdTe and CdSe high-power infrared laser window crystals.

10. A unique determination of the optical mode phonon frequencies of CdS and ZnO (at various symmetry points in the Brillouin zone), measured from their phonon-assisted, bound exciton, photoluminescence transitions at low temperature.

11. First observation of bound exciton antistokes emission line, due to a non-thermal distribution of LO-phonons at low temperature in CdS.

12. Observation of both bound and free exciton photoluminescence transitions at photon energies above the absorption edge of CdS at low temperature.

13. Observation of a bound phonon quasiparticle in CdS (optical mode phonons highly localized at a bound exciton acceptor site).

14. First observation of sharp, bound exciton photoluminescence transitions and their phonon replicas in polycrystalline ZnSe laser window crystals.

15. First observation of spin-flip-Raman scattering from electrons in the n-type CdTe, CdSe and GaAs: measurement of the effective electron g-factor in these materials.

16. Observation of acoustic-phonon-assisted cyclotron resonance absorption in semiconductors.

17. First polaron cyclotron resonance measurement of the theoretically predicted electron-phonon interaction in n-InAs (measurements performed in high mobility InAs epi-layers).

18. First magneto-spectroscopic measurement (far infrared Zeeman spectroscopy) of the characteristic shallow donor electron transitions in n-type InAs and CdTe.

19. First quantitative polaron cyclotron resonance measurement of the electron-phonon interaction in CdTe: First conclusive confirmation of Frohlich's continuum model theory of large polaron formation in polar semiconducting media.

VII   CONCLUSIONS AND RECOMMENDATIONS

This report and the publications listed in the Appendix summarize the more important aspects of the research program performed under this task. The significant achievements have been summarized separately.

The major goal of the research was to advance the "state-of-the-art" of the II-VI compound semiconductors, particularly with regard to the growth of high quality single crystals, and to the characterization of the fundamental physical properties, as well as the characterization of the electronic defect structure. This has been achieved through extensive studies of the optical and magneto-optical properties of these materials. As a consequence of the research effort, the II-VI compounds are now a very well understood class of electronic materials, although there is still much work to be done in the area of their non-linear optical properties. The development and perfection of bound exciton Zeeman spectroscopy as an analytical technique for the identification of semiconductor defects and impurities was a pioneering effort of the research program.

It is recommended that the techniques of magneto-optical spectroscopy which have been developed for the II-VI compounds be extended to the III-V compound semiconductors, for the purpose of characterizing the electronic defect structure in these materials, particularly GaAs and InP, which have considerable potential for electronic and optical device applications.

APPENDIX

List of Publications

The following is a list of publications which resulted from the research performed under Project 7885, Task 0004. This list includes publications by both in-house and contractor personnel; it is not necessarily a complete list, but is meant to be a representative list of the more significant publications generated under this Task effort during the period 1 July 1964 to 30 June 1974.

1. D.C. Reynolds and C.W. Litton, "Edge Emission and Zeeman Effects in CdS", Phys. Rev. 132, 1023 (1963).

2. C.W. Litton and D.C. Reynolds, "Double Carrier Injection and Negative Resistance in CdS", Phys. Rev. 133A, 536 (1964).

3. D.C. Reynolds, C.W. Litton and R.G. Wheeler, "The Vibrational Spectrum of a Bound Exciton Complex in CdS", Proc. of 7th Inter. Conf. on Physics of Semiconductors, Paris, 1964 (Dunod Press, Paris, 1964), p. 739.

4. T.C. Collins, C.W. Litton and D.C. Reynolds, "Semi-Empirical Calculations of the Vibrational Spectrum of a Bound Exciton Complex in CdS", Proc. of 7th Inter. Conf. on Phys. of Semiconductors, Paris, 1964 (Dunod Press, Paris, 1964). p. 745.

5. D.C. Reynolds, "Growth of Sulfides", Chapt. IV of Book: The Art and Science of Growing Crystals (John Wiley & Sons, New York, 1963).

6. D.C. Reynolds, "CdS Solar Cells for Space Applications", OAR Research Review, V.1.II, 22, Jan 1964.

7. C.W. Litton, D.C. Reynolds and T.C. Collins, "The Vibrational Spectra of a Bound Exciton Complex in CdSe", Proc. of the Hull Luminescence Conf., Hull, 1964 (Proc. of the Physical Soc., London, 1964).

8. D.C. Reynolds, "Excitons in CdS", Review Paper, J. Physical Soc. Japan Suppl. 20, 1830 (1964).

9. D.C. Reynolds, C.W. Litton and T.C. Collins, "Some Optical Properties of Group II-VI Semiconductors", Part I, Review Paper, Physica Status Solidi 9, 645 (1965).

10. D.C. Reynolds, C.W. Litton and T.C. Collins, "Some Optical Properties of Group II-VI Semiconductors", Part II, Review Paper, Physica Status Solidi 12, 3 (1965).

11. D.C. Reynolds, "Magneto-Optical Properties of Semiconducting Solids", ISA Transactions, Instrument Soc. of America 4, 1 (1965).

12. D.C. Reynolds, C.W. Litton and T.C. Collins, "Zeeman Effects in the Edge Emission and Absorption of ZnO", Phys. Rev. 140, 1726 A (1965).

13. Y.S. Park, C.W. Litton, T.C. Collins and D.C. Reynolds, "Exciton Spectrum of ZnO", Phys. Rev. 143, 512 (1966).

14. D.C. Reynolds, C.W. Litton, Y.S. Park and T.C. Collins, "Sharp Line Emission Due to Preferential Pairing in ZnO Crystals", Proc. of 8th Inter. Conf. on Phys. of Semiconductors, Kyoto, 1966 (J. Phys. Soc. Japan Suppl., Kyoto, 1966), p. 143.

15. D.C. Reynolds, "Lasing Potential of II-VI Compounds", Proc. of Air Force Science and Engineering Symposium, Sept. 1966.

16. D.C. Reynolds, C.W. Litton and T.C. Collins, "Edge Emission and Magneto-Optical Effects in CdSe", Phys. Rev. 156, 881 (1967).

17. D.C. Reynolds, "Coherent and Non-coherent Light Emission in II-VI Compounds", Trans. of the Metallurgical Soc. of AIME 239, 300 (1967).

18. C.W. Litton and D.C. Reynolds, "The Lasing Transitions of CdS", Proc. of the Inter. Conf. on II-VI Compounds, Ed. by Thomas, Providence, R.I., 1967 (Benjamin Press, New York, 1967), p. 694.

19. C.W. Litton, "Sharp Line Emission Due to Preferential Pairing in Li- and Na-Doped ZnO Crystals", Proc. of the Swansea Semicon-- ductor Conf., Swansea, England, 1966 (Proc. of the Phys. Soc., London, 1966), p. 136.

20. C.W. Litton and Y.S. Park, "Current and Light Storage in Li- and Na-Doped ZnO Crystals", Proc. of 13th Air Force Science and Engineering Symposium, Tullahoma, 1966, p. 29.

21. C.W. Litton, T.C. Collins and D.C. Reynolds, "Spatial Resonance Dispersion Effects in the Reflection Spectrum of CdSe", Phys. Rev. 164, 1035 (1967).

22. L.C. Greene and C.R. Geesner, "An Improved Furnace for the Growth and Treatment of II-VI Compound Single Crystal Platelets", J. Appl. Phys. 38, 3662 (1967).

23. Y.S. Park and D.C. Reynolds, "Growth of ZnO Single Crystals", J. Appl. Phys. 38, 756 (1967).

24. D.C. Reynolds, R.N. Euwema and T.C. Collins, "Evidence for Spatial Dispersion in Emission from CdS Platelets", Proc. 9th Inter. Conf. on Phys. of Semiconductors, Moscow, 1968 (Nauka Press, Moscow, 1968), p. 210.

25. C.J. Summers, R.B. Dennis, S.D. Smith and C.W. Litton, "Infrared Magneto-Optical Studies of Linewidth Anomalies Caused by Resonant Polaron Coupling to Magnetic States in Polar Semiconductors", Proc. of 9th Inter. Conf. on Phys. of Semiconductors, Moscow, 1968 (Nauka Press, Moscow, 1968), p. 1029.

26. Y.S. Park and C.W. Litton, "Storing Light and Current in Crystals", Electronics Magazine 41, 104 (1968).

27. D.C. Reynolds, C.W. Litton and T.C. Collins, "Excited States of Bound Exciton Complexes in CdS", Phys. Rev. 174, 3 (1968).

28. D.L. Kingston, L.C. Greene and L.W. Croft, "The Edge Emission Bands in CdS", J. Appl. Phys. 39, 12 (1968).

29. D.C. Reynolds, "Excitons in II-VI Compounds", Optical Properties of Solids, Ed. by Nudelman and Mitra, Proc. of NATO Adv. Study Institute, Freiburg, 1969 (Plenum Press, New York, 1969), p. 239.

30. D.C. Reynolds, C.W. Litton and T.C. Collins, "Excited Terminal States of Bound Exciton Donor Complexes in CdSe", Phys. Rev. 177, 1161 (1969).

31. D.C. Reynolds, "Emission from Excited Terminal States of Bound Exciton Complexes", Electronic Structure of Solids (Plenum Press, New York, 1969), p. 110.

32. D.C. Reynolds and T.C. Collins, "Emission from Excited Terminal States of Bound Exciton Complexes", Zeit. fur Naturforschung 24a, 9 (1969).

33. D.C. Reynolds and T.C. Collins, "Excited Terminal States of a Bound Exciton Donor Complex in ZnO", Phys. Rev. 185, 1099 (1969).

34. D.C. Reynolds and T.C. Collins, "Donor-Acceptor Pair Recombination Spectra in CdS Crystals", Phys. Rev. 188, 1267 (1969).

35. C.W. Litton, R.B. Dennis and S.D. Smith, J. Phys. C., Solid State Phys. (London) 2, 2146 (1969).

36. C.W. Litton and R.B. Dennis, "Infrared C.R. in Epitaxially Grown InAs Films", Solid State Comm. 8, 2015 (1970).

37. C.W. Litton, R.B. Dennis and B.S. Wherrett, "Combinational Resonance in n-CdTe", Proc. High Magnetic Fields Conf. (Nottingham Univ. Press, Nottingham, 1970), p. 53.

38. B.S. Wherrett, R.B. Dennis, C.W. Litton and S.D. Smith, "The Magneto-Optical Absorption Spectrum of Donor Electrons in CdTe", J. Phys. C, Solid State Phys. (London) 1, L59 (1970).

39. D.C. Reynolds and D.J. Stukel, "Space Flight Testing of CdS Solar Cells", Proc. NASA Conf. on Solar Batteries, NASA Lewis Labs (1970).

40. D.C. Reynolds, C.W. Litton and T.C. Collins, "Short Wavelength Impurity Exciton Transitions in CdS at 1.2°K", J. Phys. C, Solid State Phys. (London) 4, 258 (1970).

41. D.C. Reynolds, C.W. Litton, T.C. Collins and E.N. Frank, "Phonon Side Bands on the Bound Exciton Transitions in CdS and ZnO", Proc. of the 10th Inter. Conf. on Phys. of Semiconductors, Cambridge, 1970 (U.S. Atomic Energy Comm. Press, Washington, 1970), p.519.

42. D.C. Reynolds, C.W. Litton, T.C. Collins and Y.S. Park, "Exciton-Lo Phonon Interaction and the Antistokes Emission Line in CdS", Phys. Rev. Letters 25, 1619 (1970).

43. C.W. Litton, K.J. Button, B. Lax, M. Weiler and W. Dreybrodt, "Acoustic-Phonon-Assisted Cyclotron Resonance in Semiconductors", Proc. of 10th Inter. Conf. on Phys. of Semiconductors, Cambridge, 1970 (U.S. Atomic Energy Comm. Press, Washington, 1970, p. 847.

44. C.W. Litton, K.J. Button, B. Lax and W. Dreybrodt, "Acouto-Polaron in CdTe", Solid State Comm. 8, 2177 (1970).

45. D.C. Reynolds, C.W. Litton and T.C. Collins, "A Bound Exciton Quasiparticle in CdS", Phys. Rev. 4B, 1868 (1971).

46. D.C. Reynolds, C.W. Litton, T.C. Collins and Y.S. Park, "Optical Phonons Bound to Neutral Acceptors in CdS", Proc. of 1st Inter. Conf. on Phonons, Rennes, France (Dunod Press, Paris, 1971), p. 319.

47. T.W. Walker, C.W. Litton, D.C. Reynolds, T.C. Collins, W.A. Wallace, J.H. Gorrell and K.C. Jungling, "Electron Spin-Flip Raman Scattering in II-VI Compounds", Proc. 11th Inter. Conf. on Phys. of Semiconductors, Warsaw, 1972 (Polish Acad. Science, Warsaw, 1972), p. 255.

48. C.W. Litton, D.C. Reynolds, and T.C. Collins, "Strain Splitting of Bound Exciton States in CdS", Proc. 11th Inter. Conf. on Phys. of Semiconductors, Warsaw, 1972 (Polish Acad. Science, Warsaw, 1972), p. 426.

49.   C.W. Litton, D.C. Reynolds and T.C. Collins, "Γ-Point Valence Band Energy Levels in CdS Determined from Excited States of A- and B-Band Excitons", Phys. Rev. 15B, 2269 (1972).

50.   L.C. Greene and H.A. Wilson, "Edge Emission Bands in High Purity CdS", J. Appl. Phys. 42, 2758 (1971).

51.   T.W. Walker, C.W. Litton, W.A. Wallace and D.C. Reynolds, "Spin Flip Raman Scattering in GaAs and CdTe", Bull. Am. Phys. Soc., March Meeting APS, San Diego, 1972.

52.   D.C. Reynolds, C.W. Litton, D.W. Naas and D.E. Johnson, "Laser Windows: High Power Density Transmission of 10.6μm Laser Radiation Through Single Crystal CdTe and CdSe", Proc. of the Conf. on High Power Infrared Laser Window Materials, AFCR, 1971 (AFCRL Report No. 71-0592, Dec. 1971), p. 307.

53.   D.C. Reynolds, C.W. Litton, D.W. Naas and D.E. Johnson, "II-VI Crystals for Infrared Laser Windows", Proc. of Air Force Science and Engineering Symposium, San Antonio, Texas, Sept. 1972.

54.   D.C. Reynolds, C.W. Litton, D.W. Naas and D.E. Johnson, "Photoluminescent Analysis of ZnSe Laser Window Materials", Proc. of 3rd Conf. on High Power Infrared Laser Window Materials, Hyannis, Mass., 1973 (AFCR Report No. TR-74-0085 III, Feb. 1974), p. 267.

55.   D.C. Reynolds, C.W. Litton, D.W. Naas and D.E. Johnson, "Single Crystal Growth of ZnSe from the Vapor Phase", Proc. of 4th Conf. on High Power Laser Window Materials, Tucson, Arizona, 1974 (ARPA, Univ. of Dayton Press, 1974), p. 519.

56.   L.C. Greene and H.A. Wilson, "Short Wavelength Edge Emission Bands in Undoped CdS", J. Appl. Phys. 44, 5173 (1973).

57.   C.W. Litton, K.J. Button, J. Waldman, D.R. Cohn and B. Lax, "Verification of Polaron Cyclotron Resonance Theory and Determination of Coupling Constant in n-CdTe", Presented at 12th Inter. Conf. on Phys. of Semiconductors, Accepted for Publication, Solid State Comm., Sept, 1975.

58.   C.W. Litton, K.J. Button, D.R. Cohn and H.C. Praddaude, "Submillimeter Magneto-Spectroscopy in n-Type InAs Epitaxial Layers: Shallow Hydrogenic Donor Impurity States", Proc. of Inter. Conf. on Submillimeter Waves and Their Applications, Atlanta, 1974 (Transactions IEEE, Dec. 1974).

59.   M.M. Kreitman, S.P. Faile, C.W. Litton and D.C. Reynolds, "Optical Transmission in Iodine Transported HgS Cinnabar", Conf. on Optical Properties of Highly Transparent Solids, Ed. by B. Bendow, New Hampshire, 1975 (Pergamon Press, New York, 1975).

60. D.C. Reynolds, C.W. Litton and T.C. Collins, "Double-Acceptor Donor Pair Lines in CdS", Accepted for Publication, Solid State Comm., June 1975.

61. D.C. Reynolds, C.W. Litton and S.B. Nam, "Excited Terminal States of Bound Exciton Donor Complexes in n-GaAs Epi-layers", To be published, Phys. Rev. 1975.

62. H.J. Stocker, "Probable Observation of Unusual Local Vibrational Modes in the Oscillatory Photoconductivity of Semi-insulating GaAs", Solid State Comm. 16, 2134 (1975).

63. D. Kniola, T.C. Collins, S.B. Nam, D.C. Reynolds and C.W. Litton, "Intrinsic Exciton Spectra of InP and GaAs Epitaxial Layers", to be published, Phys. Rev. 1975.

64. N.E. Heyerdahl, D.J. Harvey and R.F. Belt, "Research on Photovoltaic Cells, ARL Report No. 64-142, Oct. 1964.

65. R.M. Esposito, "An Investigation of the Photovoltaic Effect Associated With a Lifetime Gradient in a Semiconductor", ARL Report No. 65-74, April 1975.

66. N.E. Hyerdahl and D.J. Harvey, "Research on Photovoltaic Cells", ARL Report No. 65-111, June 1965.

67. L.R. Shiozawa, G.A. Sullivan and F. Augustine, "Research on the Mechanism of the Photovoltaic Effect in High Efficiency CdS Thin Film Solar Cells", ARL Report No. 67-0190, Sept. 1967.

68. H.E. Nastelin, J.R. Hietanen and F.A. Shirland, "Fabrication of CdS Thin Film Solar Cells for Space Vehicle Testing", ARL Report No. 67-0282, Dec. 1967.

69. L.R. Shiozawa, F. Augustine, G.A. Sullivan, J.M. Smith and W.R. Cook, "Research on the Mechanism of the Photovoltaic Effect in High Efficiency CdS Thin Film Solar Cells," ARL Report No. 69-0155, Oct. 1969.

70. W.F. Dunn and H.E. Nastelin, "Improvements in CdS Thin Film Solar Cells", ARL Report No. 70-0036, March 1970.

71. L.R. Shiozawa, F. Augustine and W.R. Cook, "Research on the Operating and Failure Mechanisms in CdS Solar Cells", ARL Report No. 70-0169, Sept. 1970.

72. W.F. Dunn, "Improvements in CdS Thin Film Solar Cells", ARL Report No. 71-0015, Jan. 1971.

73. L.W. Brown, J.T. Buford, R.H. Fahrig, et al., "Research in Purification and Single Crystal Growth of II-VI Compounds, ARL Report No. 65-100, May 1965.

74. R.H. Fahrig, L.W. Brown and G.N. Webb, "Research in Purification and Single Crystal Growth of II-VI Compounds", ARL Report No. 67-0070, April 1967.

75. R.H. Fahrig, L.W. Brown and G.N. Webb, "Research in Purification and Single Crystal Growth of II-VI Compounds", ARL Report No. 68-0096, May 1968.

76. R.H. Fahrig, G.N. Webb and C.R. Porter, "Research in Purification and Single Crystal Growth of II-VI Compounds", ARL Report No. 70-0106, June 1970.

77. L.R. Shiozawa and J.M. Jost, "Research on Improved II-VI Crystals", ARL Report No. 67-0149, July 1967.

78. L.R. Shiozawa, J.M. Jost and G.A. Sullivan, "Research on Improved II-VI Crystals", ARL Report No. 68-0153, August 1968.

79. L.R. Shiozawa and J.M. Jost, "Research in Improved II-VI Crystals", ARL Report No. 69-0107, July 1969.

80. L.R. Shiozawa and J.M. Jost, "Research on Improved II-VI Crystals", ARL Report No. 71-0017, Jan. 1971.

81. A.J. Socha, E.M. Masumoto and R.K. Willardson, "Analytical Techniques for the Determination of Trace Impurities in II-VI Compounds", ARL Report No. 70-0170, Sept. 1970.

TABLE I

ENERGY BAND PARAMETERS OF THE II-VI COMPOUND SEMICONDUCTORS
AT LOW TEMPERATURES (20°K and below) UNLESS OTHERWISE INDICATED
(After Reynolds, Litton and Collins)

Material	Crystal Structure	Bandgap E_G (eV) $\Gamma_7-\Gamma_9$ or $\Gamma_6-\Gamma_8$	Valence Band Separations	
			E_{AB} (eV) $\Gamma_9-\Gamma_7$ or $\Gamma_8-\Gamma_7$	E_{BC} (eV) $\Gamma_7-\Gamma_7$
CdS	Wurtzite	2.582	0.016	0.057
ZnS	Wurtzite	3.910	0.029	0.082
ZnS	Zincblende	3.84	0.065	
ZnO	Wurtzite	3.436	0.006	0.038
CdSe	Wurtzite	1.840	0.025	0.407
ZnSe	Wurtzite	2.795[1]	0.046[1]	
ZnSe	Zincblende	2.83	0.41	
ZnTe	Znicblende	2.39	0.91	
CdTe	Zincblende	1.607	0.81	
α-HgS	Trigonal (Cinnabar)	2.25		
β-HgS	Zincblende	-0.15[1][2]		
HgSe	Zincblende	-0.2[2]		
HgTe	Zincblende	-0.025[2]		

Note: References to original sources of this data can be found in
Reynolds, Litton and Collins, Refs. 9 and 10.

(1) Denotes room temperature value.

(2) β-HgS, HgSe and HgTe are semimetals and have the equivalent of
negative bandgaps. Harman has reviewed evidence that these
materials have the peculiar inverted band structure of grey
tin (T. C. Harman, Phys. and Chem. of II-VI Compounds, North
Holland Pub., 1967, p. 767).

TABLE II

DIELECTRIC PARAMETERS OF THE II-VI COMPOUND
SEMICONDUCTORS AT ROOM TEMPERATURE
(After Reynolds, Litton and Collins)

Material[1]	Dielectric Constant		Refractive Index
	ε_s	ε_∞	n
CdS(w)	$\varepsilon_{33}^T/\varepsilon_0$ - 10.33	5.24	2.30 ($\lambda=2\mu m$)
	$\varepsilon_{11}^T/\varepsilon_0$ - 9.35		
	$\varepsilon_{11}/\varepsilon_0$ - 9.02		
ZnS	$\varepsilon_{11}^T/\varepsilon_0$ - 8.32	5.13	2.26 ($\lambda>2$ m)
ZnO(w)	ε_z - 8.87	4.59	2.14
	ε_x - 8.47		
CdSe(w)	$\varepsilon_{11}^T/\varepsilon_0$ - 10.65	7.02	2.55 ($\lambda=0.85\mu m$)
	$\varepsilon_{33}^T/\varepsilon_0$ - 9.70		
	$\varepsilon_{11}^5/\varepsilon_0$ - 9.53		
ZnSe(z)	$\varepsilon_{11}^T/\varepsilon_0$ - 9.1	5.75	2.57 ($\lambda=0.64\mu m$)
ZnTe(z)	$\varepsilon_{11}^T/\varepsilon_0$ - 10.1	8.26	2.77 ($\lambda=1.24\mu m$)
CdTe(z)	$\varepsilon_{11}^T/\varepsilon_0$ - 9.6	7.13	2.83 ($\lambda=1\mu m$)
HgTe(z)	20	14	3.7 ($\lambda>80\mu m$)

Note: References to original sources of this data can be found in
Reynolds, Litton and Collins, Refs. 9 and 10.

(1) Wurtzite and Zincblende structures are denoted by (w) and (z),
respectively.

TABLE III

OPTICAL MODE PHONON ENERGIES (FREQUENCIES) OF THE II-VI COMPOUND SEMICONDUCTORS AT ROOM TEMPERATURE (300°K) UNLESS OTHERWISE INDICATED (After Reynolds, Litton and Collins).

Material[1]	LO Phonon		TO Phonon	
	Energy (eV)	Frequency (cm^{-1})	Energy (eV)	Frequency (cm^{-1})
CdS(w)	$0.0376^{[2]}$	$303.5^{[2]}$	$0.0288^{[2]}$	$232.5^{[2]}$
ZnS(w)	0.044	355	0.036	290
ZnS(z)	0.042	340	0.037	298
Zno(w)	$0.0713^{[2]}$	$575.5^{[2]}$	$0.0486^{[2]}$	$392^{[2]}$
CdSe(w)	0.027	218	0.023	185
ZnSe(z)	0.031	250	0.026	210
ZnTe(z)	0.0259	209	0.0236	190
CdTe(z)	$0.0212^{[2]}$	$171.0^{[2]}$	$0.0180^{[2]}$	$145.0^{[2]}$
$\propto$-HgS	$0.0426^{[2]}$	$344^{[2]}$	$0.0356^{[2]}$	$287.5^{[2]}$
HgTe(z)	0.017	138	0.014	115

Note: References to original sources of this data can be found in Reynolds, Litton and Collins, Refs. 9 and 10.

(1) Wurtzite and Zincblende structures are denoted by (w) and (z), respectively

(2) Denotes low temperature values (below 20°K).
The values given for Cds and Zno are the averages of the TO, and TO_2
and the LO_1 and LO_2 values as determined from bound exciton photoluminescence spectra (See Ref. 41).

TABLE IV

TYPICAL VALUES OF THE OPTICAL MODE PHONON FREQUENCIES AT THE Γ-SYMMETRY POINT IN CdS and ZnO, CALCULATED FROM PHONON DISPERSION THEORY AND BOUND EXCITON SPECTRAL EMISSION DATA.

Symmetry	Mode	CdS $\nu\tau(cm^{-1})$	ZnO $\nu\tau(cm^{-1})$
Γ_5	LO_1	304.6	581.4
Γ_1	LO_2	302.2	570.4
Γ_6		257	444
Γ_5	TO_1	240	413
Γ_1	TO_2	228	380

Note: After Reynolds, Litton, Collins and Frank, Ref. 41.

TABLE V

INTRINSIC EXCITON PARAMETERS OF II-VI COMPOUND SEMICONDUCTORS
AT LOW TEMPERTURE (20°K and Below). After Reynolds, Litton and Collins

Material(1)	A-exciton ground state energy (ev)	E_B (eV) Exciton Binding energy	μ^*ex (2) Exciton reduced mass	M^*h (2) Hole effective mass	M^*e (2) Electron Effective mass	a_0 Radius of Bohr orbit (Å)
CdS(w)	Γ5L (4853Å) 2.5537 Γ5T (4854.5Å) Γ6 (4857Å)	0.028	0.18	∥ 5 ⊥ 0.7 ± 0.1	0.171 ⊥ 0.153 ∥	27
ZnS(w)	3.8714	0.036	0.18 ± 0.01	⊥ 0.58 ± 0.1	∥ 0.28 ± 0.03 ⊥ 0.27 ± 0.03	21
ZnO(w)	3.3768	0.059	0.31	1.8	0.38	14
CdSe(w)	1.8258	0.0157	0.13 ± 0.01	∥ > 1 ⊥ 0.45 ± 0.09	0.13 ± 0.01 (isotropic)	54
ZnSe(z)	2.799	0.019	0.105	0.6	0.1	
ZnTe(z)	2.381	0.010				
CdTe(z)	1.595	0.012	0.071			

Note: References to original sources of this data can be found in Reynolds, Litton and Collins, Refs. 9 and 10.

(1) Wurtzite and Zincblende structures are denoted by (w) and (z).

(2) Data for exciton, hole and electron effective masses are given in units of electron rest mass, m_0.

TABLE VI

SOME CHARACTERISTIC BOUND EXCITON PHOTOLUMINESCENCE LINES OBSERVED IN CdS AT LOW TEMPERATURE (T ~ 1.2°K).

Line	Polarization	Energy (eV) [(Å)]	Line Width (meV)	Energy below A-exciton (2.5537eV) (eV)	Energy below B-exciton (2.5687eV) (eV)	Type of Exciton Complex
I_1	$E \perp c$	2.53585 (4888.47)	0.1	0.0177		Neutral acceptor
I_2	$E \perp c$	2.54695 (4867.17)	0.1	0.0066		Neutral donor
I_{1B}	$E \parallel c$	2.54887	0.1		0.0198 ⎤	Neutral acceptor (B-band exciton)
I_{1B}	$E \perp c$	2.54914	0.1		0.0196 ⎦	
I_3	$E \perp c$	2.54984 (4861.66)	0.1	0.0038		Ionized donor (zero-field split)
I_3	$E \perp c$	2.54953 (4862.25)	0.1			
I_5	$E \perp c$	2.54592 (4869.14)	0.1			Neutral acceptor
I_6	$E \parallel c$	2.44576	0.1			Zero-field split
I_6	$E \parallel c$	2.44576	0.1			

Note: Original data is from Thomas and Hopfield and Reynolds, Litton and Collins; Collected in review of Refs. 9 and 10.

TABLE VII

SOME CHARACTERISTIC BOUND EXCITON PHOTOLUMINESCENCE LINES
OBSERVED IN CdSe AT 1.2°K.

Line	Wavelength (A)	Energy (eV)	Preferential Polarization	Intensity	Splitting	g-value
I_1	6790.95	1.8254	$E \perp C$	Weak	Doublet	0.52
I_2	6792.60	1.8250	$E \perp C$	Weak	Doublet	0.52
I_3	6794.12	1.8246	$E \perp C$	Weak	Doublet	0.52
I_4	6804.18	1.8219	$E \perp C$	Very Strong	Multiplet	----
I_5	6805.85	1.8214	$E \perp C$	Strong	Doublet	0.53
I_6	6821.84	1.8172	$E \perp C$	Strong	Doublet	0.53
I_7	6827.43	1.8157	$E \perp C$	Strong	Quartet	1.96/0.50
I_{8a}	6846.62	1.8106	$E \perp C$	Weak	Complex	

Note: After Reynolds, Litton and Collins, Ref. 16.

74

TABLE VIII

COMPARISONS OF ELECTRON g-FACTORS DETERMINED FROM
SPIN-FLIP RAMAN SCATTERING AND SEVERAL OTHER METHODS
IN SEVERAL WIDE BANDGAP MATERIALS (T < 20°K).
(After Walker, et al., Ref. 47).

Material	Present Spin-Flip Raman	NMR	Other Methods
Cds	1.76 ± 0.04	1.56 ± 0.12	1.78 EPR
			1.74 Exciton Magneto Optics
			1.76 SFR
CdSe	0.53 ± 0.03	0.53 ± 0.04	0.54 Exciton Magneto Optics
			0.52 Exciton Magneto Optics
			0.68 EPR
CdTe	0.75 ± 0.03	-1.09 ± 0.10	-0.47 K.P calculation
GaAs	0.53 ± 0.03		0.52 EPR
			-0.43 Exciton Magneto Optics